Unterschrift des Betreuers

DIPLOMARBEIT

CONTRIBUTIONS TO THE BELLE II SENSOR DEVELOPMENT AND QUALIFICATION

ausgeführt am

Institut für Hochenergiephysik
der Österreichischen Akademie der Wissenschaften

ausgeführt von

Lorenzo de Cillia B.Sc
Tandelmarktgasse 20/10
1020 Wien

unter der Anleitung von

Univ.Doz. Dipl.-Ing. Dr.techn. Manfred KRAMMER und
Dipl.-Ing. Dr. techn. Thomas BERGAUER

5.12.2014

Unterschrift des Verfassers

Abstract

The given master thesis was carried out at the Institute of High Energy Physics of the Austrian Academy of Sciences [1] in Vienna. It treats the quality management of the double-sided, trapezoidal strip sensors that are used for the SVD (Silicon Vertex detector). The SVD will be one of the particle detectors used in the Belle II project in Tsukuba, Japan that starts in 2016. In total, the SVD consists of 4 detector layers that are made out of 187 double-sided strip sensors. Beside the 60 trapezoidal sensors that were produced by Micron Semiconductors, 127 double-sided rectangular sensors (produced by Hamamatsu Photonics K.K.) build the SVD. The SVD composes (together with the Pixel detector PXD) the Vertex detector (VXD) aiming to reconstruct the vertices of the collided particles. The particle accelerator that is associated to the Belle II project is the asymmetric electron-positron collider SuperKEKB. The Belle II experiment is the successor of the Belle experiment. Its outputs resulted in a won Nobel Prize for Kobayashi and Maskawa (2008) and over 300 publications in physics journals.

To assure a sufficient quality of the sensors building the SVD, HEPHY and Micron Semiconductors arranged strict mechanical and electrical specifications for the delivered sensors. Those parameters were determined either for each strip (512 or 768 strips, depending on the side) or globally for the whole sensor. In contrary to the rectangular sensors (that were tested by Hamamatsu before the shipping), one part of the trapezoidal Micron sensors was measured at HEPHY Vienna- the other part was measured at the National Institute of Nuclear Physics (INFN) in Trieste. At the Quality Testing Center (QTC) in Vienna the author measured the significant parameters (on both sides) and then compared them to the specifications. After evaluating the measurement results, the author divided the sensors into three classes of quality. Sensors with the lowest grade C are used as mechanical dummies, sensors with the medium grade B are electrically functional and will be mostly used for prototypes and tests, whereas sensors with the best grade A have the highest quality and will be used in the Belle II project. After dividing the sensors into those three classes, the measurement results were statistically analyzed by the author. Histograms were plotted to see if the measured quantities depend on the batch number in order to find out if there was a possible link between the sensor quality and the date of construction. Not only the 32 sensors that were measured at HEPHY but also the 24 sensors from Trieste were statistically analyzed by the author and it was sought for systematic differences in the results, in order to identify potential systematic errors or biases of both measurements. Also the quality of the Viennese sensors were compared to those measured in Trieste.

So, all in all, the task of this master thesis project was to qualify or disqualify the double-sided trapezoidal Micron sensors for the Belle II project. To summarize, the measurement results were satisfactory. From the 56 measured trapezoidal Micron sensors, 43 were accepted and 13 rejected. In the SVD grading system 31 sensors were rated with A, 19 sensors with B and 6 sensors with the grade C.

Kurzfassung

Die vorliegende Masterarbeit wurde am Institut für Hochenergiephysik (HEPHY) der österreichischen Akademie der Wissenschaften [1] in Wien durchgeführt. Der Verfasser widmete sich dabei dem Qualitätmanagement für die doppelseitigen, trapezoiden Streifen-Sensoren, die den Silicon Vertex Detector (SVD) bilden werden. Der SVD ist ein Teil des ab 2016 laufenden Belle II Experiments in Tsukuba, Japan. Zusammen mit dem Pixel Detector (PXD) bildet er den Vertex Detector (VXD), der das Ziel hat die Vertices der kollidierten Teilchen zurückzuverfolgen. Der Silicon Vertex Detektor besteht aus vier Lagen und im Ganzen aus 187 doppelseitigen Streifen-Sensoren. Abgesehen von 60 trapezoiden Sensoren, besteht der SVD noch aus 127 rechteckigen Sensoren. Betrieben werden die Belle II Detektoren am asymmetrischen Elektron/Positron- Beschleuniger SuperKEKB. Das Belle II Experiment ist der Nachfolger des Belle Experiments, dessen Ergebnisse 2008 in einem Nobelpreis für Kobayashi und Maskawa resultierten und in dessem Rahmen insgesamt über 300 Publikationen in Physikjournals erschienen sind.

Um die ausreichende Qualität der verbauten trapezoiden Sensoren zu garantieren, einigten sich das HEPHY und der Hersteller Micron Semiconductors auf strikte mechanische und elektrische Spezifikationen für die zu liefernden Sensoren. Im Gegensatz zu den rechteckigen Sensoren (die noch vor der Lieferung von Hamamatsu Photonics K.K. getestet wurden), wurden die trapezoiden Sensoren zum Teil vom Autor am HEPHY in Wien und zum anderen Teil am Istituto Nazionale di Fisica Nucleare (INFN) in Triest getestet. Bei den Tests in Wien und Triest wurden Sensorparameter gemessen, die für die Funktionalität der Sensoren zentral sind, und diese wurden darauf mit den vorab festgesetzten Spezifikationen verglichen. Je nachdem in welchem Ausmaß die Sensoren den Spezifikationen genügten, wurden sie dann vom Autor in drei verschiedene Qualitätsklassen eingeteilt. Die Sensoren, die am schlechtesten abschnitten (Note C), werden als elektrisch nicht funktionale, mechanische Prototypen verwendet. Die mittelgut bewerteten Sensoren (Note B) dienen als elektrisch funktionale Prototypen, die für Testbeams verwendet werden. Für das Belle II Projekt werden vorwiegend Sensoren der höchsten Güteklasse A verwendet. Um eine Entscheidungshilfe für die Einteilung in die Klassen zu bekommen, wurden die Messresultate vom Autor mit statistischen Methoden ausgewertet. Unter anderem wurde die Qualität der verschiedenen Batches verglichen. Nicht nur die insgesamt 32 am HEPHY getesteten Sensoren, sondern auch die Ergebnisse der 24 Sensoren aus Triest wurden vom Autor statistisch analysiert. Weiters wurde ein Augenmerk auf systematische Unterschiede zwischen den Messungen in Triest und Wien gelegt und die Qualität der Wiener Sensoren mit jenen aus Triest verglichen.

Die Hauptaufgabe dieser Masterarbeit bestand darin, die trapezoiden Micron Sensoren durch elektrische Messungen für das Belle II Projekt zu qualifizieren und zu charakterisieren. Die Ergebnisse der Tests waren im Großen und Ganzen zufriedenstellend. Von den 56 vermessenen trapezoiden Micron Sensoren wurden 43 akzeptiert und 13 abgewiesen. In dem SVD Bewertungssystem wurden 31 mit der Note A bewertet, 19 Sensoren mit der Note B und 6 mit der Note C.

Contents

1. The Belle experiment

1.1. Physics motivation

In the Belle II experiment rare particle decays are observed in which the physicists are looking for tiny deviations from the standard model of physics. In contrary to the LHC experiment at CERN in Geneva, where new physics is sought for on the high energy level, the Belle II project is searching for it on a high precision level. So maximum precision is one of the main challenges in the experiment.

One of the biggest scientific questions of today's physics is the observed asymmetry between antimatter and matter in our universe. An antiparticle has the exact same physical properties than the particle except of contrary charge and magnetic moment. A good example is the positron which is the antiparticle of the electron- its mass, life time and spin is equal- but in contrary to the electron it is positively charged. If matter and antimatter encounter, they convert into energy following Einstein's famous equation $E = mc^2$ and annihilate. As mentioned before, the universe seems to consist of much more matter than antimatter - e.g. all the so far observed celestial bodies are made of matter. The theory of the big bang although predicts a symmetric formation of matter and antimatter. So where does this imbalance in our universe come from?

One of the theories to explain this asymmetry is based on the so-called CP-violation. To understand what CP-violation is, we will first have to explain the concept of CP-invariance. The law of CP-invariance (in which C stands for charge conjugation and P stands for parity) claims that the physics of a system remains equal if a particle is replaced by its antiparticle (only the electrical charge changes its sign, charge conjugation symmetry) and the spatial coordinates are inverted (P symmetry). This given law although has been falsified by observation, the universe is not CP invariant. In 1964 James Cronin and Val Fitch (Nobel Prize 1980) observed a tiny anomaly to the CP invariance in the decays of neutral kaons. Nevertheless the violations so far were not sufficient to explain the predominant existence of matter to antimatter. One of the main objectives of the Belle II experiment is to gain a better understanding of this asymmetry. And the Belle physicists have already had their successes: In 2001 the first CP-violation outside of the kaon system was observed at the Belle experiment (precursor of the Belle II experiment) in the decay of B mesons. In 2008 Makoto Kobayashi and Toshihide Maskawa received the Nobel Prize of Physics for explaining the broken symmetry in the decay of kaons and for postulating a third quark family or as declared by the Nobel Prize committee "for the discovery of the origin of the broken symmetry which predicts the existence of at least three families of quarks in nature" [2]. A result of their work is the Cabibbo–Kobayashi–Maskawa matrix defining the mixing parameter between quarks.

A small excursus to better understand B hadrons that are produced in the Belle II experiment. Hadrons are particles that interact with the strong force. They consist of quarks that can (because of the quark confinement) never be observed separately. The family of hadrons consists of the baryons (consisting of three quarks) and the mesons (consisting of two quarks, a quark and an anti-quark). An often used term for the matter-antimatter asymmetry is the baryon asymmetry. Mathematically it can be expressed by the formula $\eta = \frac{n_B - n_{B'}}{n_\gamma}$, whereas n_B is the number of baryons, $n_{B'}$ the number of antibaryons and n_γ the number of photons in the universe. The observed value of the baryon asymmetry is $\eta = (6.01 \pm 0.3) \cdot 10^{-10}$ and was calculated using the cosmical background radiation.

The physics the Belle II analysis group is exercising is called B physics. It is the sector of particle physics that is about the research of hadrons which include one bottom quark. B mesons consist of a heavy bottom quark (m=4.18 GeV/c^2) and a light up-type quark and can be described much easier than mesons that consist of quarks with similar masses. Therefore the predictions that can be made are much more precise. In a B meson the bottom quark decays due to the weak interaction to an up-type quark and it is known that these types of processes violate the CP-symmetry. Another advantage of B mesons is that they can easily be produced in lepton colliders like the KEKB (the former collider of the Belle experiment). To obtain a B factory (a collider that primarily produces B mesons) the beam energy is selected so that excited Y mesons are produced that are only slightly above the necessary energy to produce a B meson and its antiparticle. Therefore they decay almost exclusively into B mesons. The SuperKEKB at the Belle II experiment will also be such a B factory. Another practical feature is that those mesons have a relatively long life time of approximately 10^{-12} s and can therefore be measured. Today a huge effort is taken to investigate charge-parity conjugation symmetry violation ("CP violation"). The so-called Standard Model (SM), which is the theory describing the interactions between elementary particles – is one of the best verified physics theories ever. It includes three of the four known fundamental forces of physics, the weak interaction, the strong interaction and the electromagnetic force. Only the gravitation isn't a part of the Standard Model (SM). The SM is a very well verified theory and enables very precise predictions. Nevertheless there are basic questions which aren't answered by the SM. For example the explanation why there are exactly three generations of elementary fermions (electrons, muons and tauons) is missing. Another unanswered question is the value of the fermions' and the bosons' masses- they are external parameters of the theory that have to be determined experimentally. The origin of mass, in the SM, is explained by the spontaneous breaking of the electro-weak symmetry. This breaking of symmetry is described similarly to a ferromagnetic material that is magnetized. When a magnet approaches the material, suddenly all internal magnetic poles align themselves into one direction and the former random orientation of the magnetic poles (symmetry) is broken.

The symmetry breaking mechanism of the electro-weak force predicts the Higgs boson. Its mass (that has been determined at approximately 125 GeV/c^2 at the LHC) is an external parameter of the theory. The SM is a very successful and accurate phenomenological concept, but physicists are still looking for some underlying theory to explain the observed discrepancies and phenomena. There are some complementary theories and concepts that account for these problems, for example the concept of supersymmetry (SUSY) and the so-called string theories, which though require additional spatial dimensions (that however cannot be perceived). These and other theories beyond the SM predict new fundamental particles and processes. Today's particle physics (respectively high energy physics) tries to generate those particles and processes either by pushing up the energy limits or it tries to find new physics by looking at tiny deviations from the SM predictions. Thus it looks for physics beyond the SM at two borders: the energy and the rare/precision border. An example for the research on the first frontier is the large energy particle collider LHC at CERN with the experiments CMS and ATLAS, an example for the second frontier will be the B-factory SuperKEKB and the Belle II experiment.

1.2. KEK

KEK [3] stands for High Energy Accelerator Research Organization, the national Japanese organization that is operating the largest particle physics laboratory in Japan. Established in 1971, it is situated in Tsukuba, Ibaraki prefecture. The KEK employs approximately 900 people, most of whom are physicists. There have been numerous experiments at KEK by internal and international collaborations, the biggest is the Belle experiment.

1.3. SuperKEKB

The SuperKEKB (see figure 1.1) is the upgraded KEKB accelerator (using the same tunnel) that is used in the Belle II experiment.The SuperKEKB is a B-factory which provides very good possibilities to study and measure the CP violation. SuperKEKB is an asymmetric electron-positron collider, where the beam energy of the electrons is 7 GeV and that of the positrons is 4 GeV. This results in a centre-of-mass energy that is very close to the mass of the excited $\Upsilon(4S)$ meson, which almost exclusively decays in B-mesons. In the SuperKEKB a linear accelerator accelerates the electrons and the positrons to their maximal energy and they are then pumped into two rings, one ring for the electrons (high energy ring, HER) and the other one for the positrons (low energy ring, LER). The circumference of the rings is 3016 m and they cross each other at the point where the Belle II experiment is located. Whereas the luminosity of the Belle experiment was $L=10^{34}$ cm^2s^{-1}, the upgraded peak luminosity of the Belle II experiment will be $8\times10^{35}cm^{-2}s^{-1}$. This will be a new world record which is a good precondition, since high luminosity and the resulting big amount of data is one of the major aspects when it comes to getting good research results in high energy physics. At the SuperKEKB there is a new nano-beam design implemented, with a smaller beam size at the interaction point. The luminosity can be written as in formula 1.1. Here, N_1 and N_2 are the numbers of particles in bunches 1 and 2 that collide, n is the number of bunches, f is the repetition frequency of collisions and A is the cross section of the bunches. More information about the SuperKEKB can be found in [4].

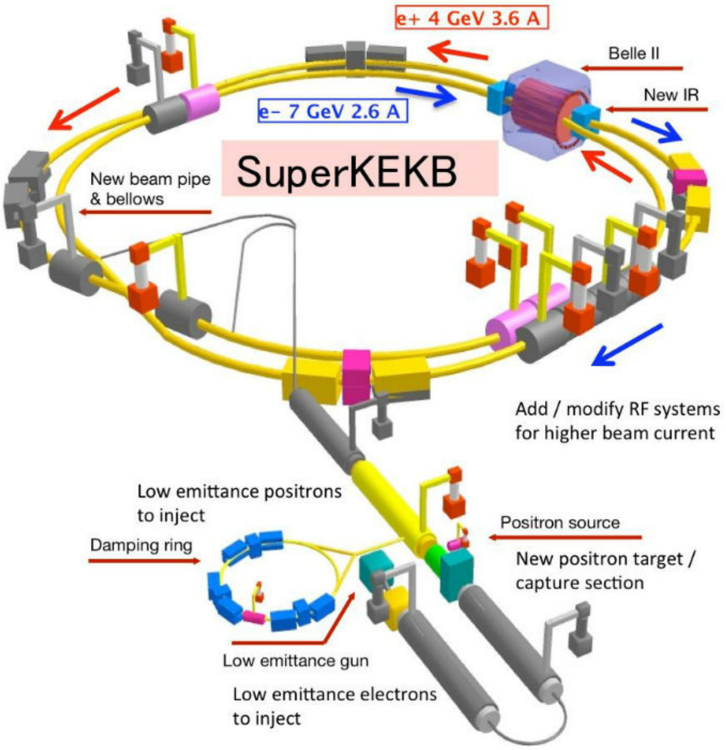

Figure 1.1.: The upgrades from the KEKB to the SuperKEKB collider. [4]

$$L = \frac{nN_1N_2f}{A} \tag{1.1}$$

1.4. Belle II

As mentioned in the former sections, Belle II is the upgrade of the Belle experiment in Tsukuba, Japan that was first presented in 2004. More than 400 physicists and engineers are working on the Belle II project. The Belle II detector is situated at the collision point of the SuperKEKB (see section 1.3), an asymmetric electron-positron collider. The Belle II detector is built out of several subdetectors, it is a multilayer particle detector. At the former Belle rare decays were intensively studied, exotic particles were sought for and precision measurements of B mesons, D mesons, and τ particles were carried out.

1.4.1. Major components

The major components of Belle II are:

- **The DEPFET Pixel Detector (PXD):** it consists of two layers of silicon pixel detectors. Its goal is to reconstruct the decay vertices of the B mesons at a very high precision.
- **The Silicon Vertex Detector (SVD):** it consists of four layers of double-sided silicon micro strip sensors. As the PXD it aims to precisely reconstruct the decay vertices of the B mesons.
- **The Central Drift Chamber (CDC):** a large gaseous detector, acting as main detecting device, measuring the tracks and momenta of the decay products.
- **Silica-Aerogel Cherenkov Counter (ACC):** it is used for particle identification, e.g. to distinguish between pions and kaons.
- **Time-of-Flight Counters (TOF):** the TOF uses plastic scintillators to identify particles by measuring their velocities and providing accurate timing signals for triggering and gatering.
- **Electromagnetic Calorimeter (ECL):** the ECL is built out of thallium-doped caesium iodide crystals that detect photons, electrons and positrons and measure their energy and positions.
- **Superconducting Solenoid:** the Superconducting Solenoid provides a magnetic field of 1.5T along the beam axis. It spans over all detector systems except the KLM. The coil wire is made of superconducting NbTi alloy and is cooled to 5K using liquid helium.
- **Kaon and Muon Detection System (KLM):** the KLM is the outermost system, consisting of alternating layers of 4.7 cm thick iron plates and active detector elements. The iron plates are used as the magnetic flux return for the solenoid. The KLM is located outside the Superconducting Solenoid and detects muons and long-lived kaons and distinguishes between them.

2. The Belle II Silicon Vertex Detector (SVD)

2.1. General information

The so called Belle II Silicon Vertex Detector (SVD) is (together with the PXD) responsible for reconstructing the vertices and the secondary vertices in the Belle II experiment. At the world record luminosity of the SuperKEKB there will be a bigger number of events, but also a higher background, which leads to more radiation damage for the SVD, more occupancy and fake hits. There will be also a higher event rate, therefore we will need a higher rate trigger, data acquisition and computing. The SVD consists of four layers of double-sided silicon strip detectors. The goal of the SVD and the PXD is to measure the two B decay vertices. The SVD has to be very light to prevent multiple scattering. Furthermore it has to be highly precise and needs a high vertex resolution. The SVD has to be radiation tolerant and mechanically stable. Its mechanical details can be found in [5]. In addition it has to be efficiently cooled and must reliably operate over a lifetime of at least ten years. Details about the cooling can be found in [6]. The SVD's outer diameter is 270 mm and it surrounds the PXD. It is equipped with double sided silicon detectors (DSSD) that are made of 6" wafers. Instead of a cylindrical design, an asymmetrically lantern shaped geometry was used to keep sensor and channel count as well as the material use as low as possible.

2.2. Main characteristics

Some main characteristics of the Belle II SVD are:

- The SVD is based on silicon micro strip sensors to avoid a large number of readout channels (compared to a pixel detector).
- The "sensor on rib" design was chosen, the sensors are glued to so called ladders.
- The inner radius is 38 mm and the outer radius 140 mm. Those values are determined by the radii of the PXD and the CDC.
- The full angular acceptance between 17° and 150° is covered.
- Tracks that are reconstructed in the CDC can be highly efficiently extrapolated to the PXD.

- The reconstruction of charged paths is improved.
- There will be 187 silicon sensors arranged in 49 ladders and the active silicon area will be 1.24 m^2. 60 of those sensors are trapezoidal and 127 are rectangular.
- A CO_2 cooling system is employed to dissipate the heat load (see [5]).
- The hit occupancy must be lower than 10%. This is necessary that reconstructed tracks in the CDC can be associated with correct hits in the vertex detector. Information from the SVD can be used to eliminate background hits in the Pixel Detector.

Image 2.1 shows the four SVD layers. The SVD layers are layers 3-6, the layers 1 and 2 are the Pixel detector. For both the SVD and the PXD they are arranged in so-called ladders. For the PXD there are in total 20 ladders, the SVD consists of 45 ladders. The silicon strip detectors are arranged cylindrically around the collision point to measure the tracks of the particles. As can be seen on the image, for the SVD there are three different designs of sensors. The large rectangular DSSD (Double Sided Silicon Detector) (green) and the narrow rectangular DSSD (blue) are used in the barrel part of the detector. The trapezoidal (Micron) DSSD (orange) is used in the forward part of the SVD.

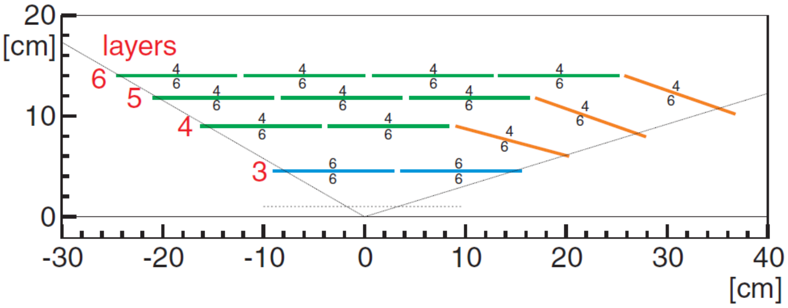

Figure 2.1.: Layers 3-6 of the Silicon Vertex Detector. [7]

The detectors used in the Belle II experiment are Double Sided Silicon Detectors (DSSD). In chapter 3.9 the basic scheme of a DSSD (see figure 3.4) and their advantages and disadvantages in comparison to one-sided detectors are explained. The design of the silicon microstrip sensors in the Belle II project is determined by the need of a small material budget. The bulk-material of the DSSD is n-type and they have a thickness of approximately 300μm. One of the main problems of the Belle II experiment is multiple scattering: Since the center-of-mass energy of the Belle II experiment will be at 10.6 GeV and so about three orders of magnitude smaller than that of the LHC (maximum center-of-mass energy of about 13 TeV), this is a much bigger issue. Due to their lower energy the particles are more easily deflected by coulomb interaction with the detector material. To reduce the multiple scattering the material used has to be as little as possible. That is why the biggest available sensors are used - the 6" inches wafers are about 12 cm long and have a width of about 6 cm. This reduces the overall amount of structural elements and thus the material budget.

In order to achieve a light-weight ladder construction with integrated readout electronics, CO_2 - cooling and a high signal-to-noise ratio, the ’Origami chip-on-sensor concept’ was developed. Depending on the layer, up to five sensors build one ladder. The structure of those ladders are two ribs made of an Airex styrofoam core with thin plies of carbon fiber laminated onto the side. The composite is very light-weight but also very stiff. The ladder design only accounts for 0.55 % of the radiation length .

2.3. Sensor producers

The two producers of the sensors are

- Hamamatsu Photonics K.K. (HPK), located in Hamamatsu City, Japan that produce the rectangular sensors for the barrel part of the SVD.
- Micron Semiconductor Ltd., located in Lancing, UK which are manufacturing the trapezoidal sensors that are used in the forward part of the SVD.

2.4. Sensor geometry

Two different kinds of barrel sensors will be produced by Hamamatsu Photonics, the barrel sensors used in layer three of the SVD are smaller than the ones used in layer 4-6. Figure 2.2 shows the geometric dimensions of the rectangular Hamamatsu sensors of layers 4-6.

As mentioned, the forward part of the SVD is built out of trapezoidal sensors in order to cover the full acceptance region while using a minimum of material. Figure 2.3 shows the geometrical dimensions of the trapezoidal sensors.

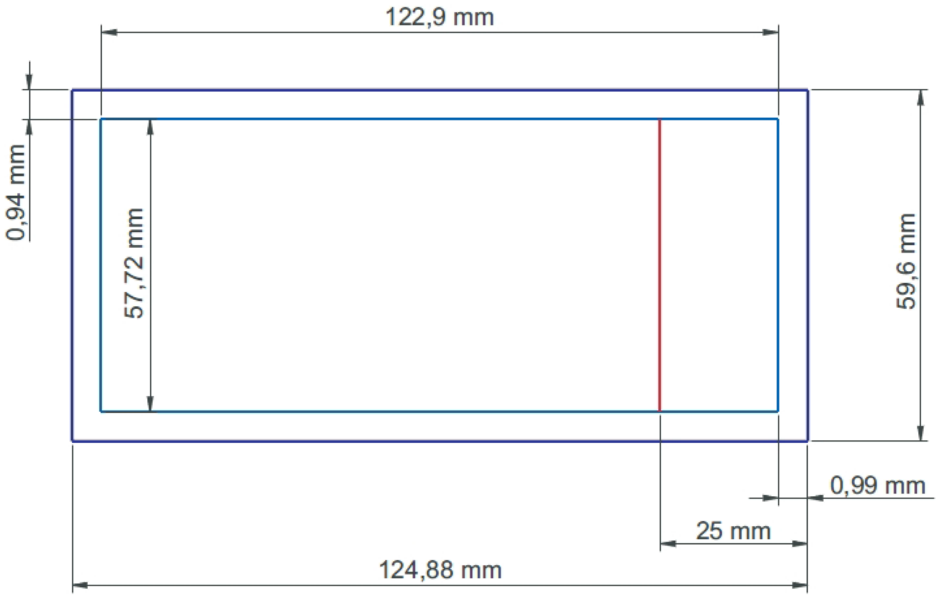

Figure 2.2.: Geometrical dimensions of the rectangular sensors of layer 4-6. [7]

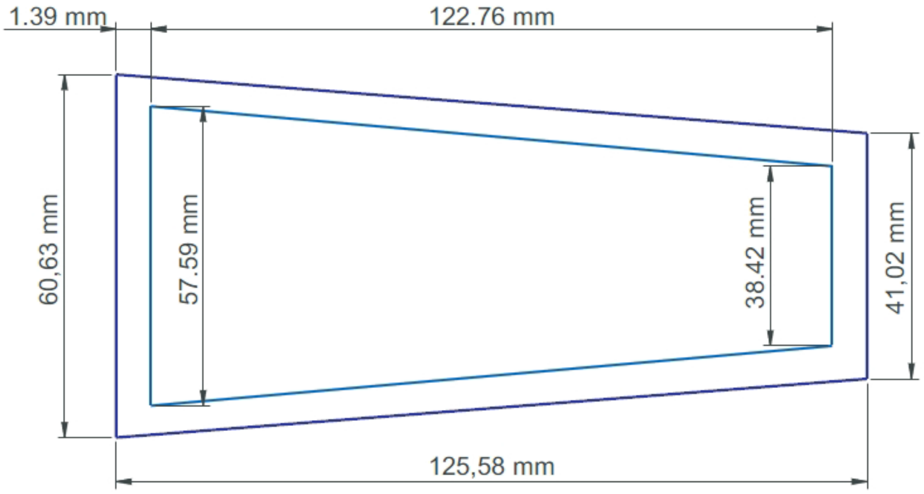

Figure 2.3.: Geometrical dimensions of the trapezoidal sensors. [7]

3. Basics of semiconductor detectors

Semiconductors have special properties that make them very suitable for the detection of ionizing radiation. They have a unique electric conductive behavior that is somewhere between that of a metal and an insulator. Semiconductor detectors are used in nuclear physics, particle physics, satellite experiments and industrial applications.

3.1. Advantages of semiconductor detectors

There is a bunch of advantages in the use of semiconductor detectors. First of all they have a high density- that implies that particles will loose a lot of energy in a short distance and diffusion is not as disturbing as in gas detectors. This leads to a very good position resolution (<10 μm). Moreover, they have a low ionization energy (a several eV per electron-hole pair and so one order of magnitude smaller) in comparison to gas detectors and scintillators. Furthermore, for semiconductors (mainly silicon) there is the micro-chip technology that has already collected a lot of experience. Since the read out electronics are made also from silicon, the integration is considerably facilitated. Despite of the high density of the material, electrons and holes can move almost freely in the material- so charge can be rapidly collected (10 ns) and detectors can be used in high-rate environments. Moreover the mechanical rigidity of silicon is very high, which allows to construct self-supporting structures.

3.2. Disadvantages of semiconductor detectors

The disadvantages are that there is no internal amplification of a small signal and also the high costs of semiconductor detectors. More disadvantages include the facts that there is a high number of readout channels resulting in a large power consumption that requires cooling.

3.3. Use of particle detectors

What goal do we want to reach by using particle detectors? The biggest goal is to track particles (as precisely as possible) while disturbing them as little as possible. Another aim is determining the position of the primary interaction vertex and of secondary decays. To accomplish this objective we need a superb position resolution, a large signal, a thin detector that is close to the interaction point and of low mass (to minimize multiple scattering).

3.4. Silicon

Silicon belongs to group IV in the periodic table of elements and has the atomic number 14. Group IV means that it has four electrons in the valence shell available for covalent bonds. Silicon is a semiconductor at room temperature. It is used in the micro electronics industry and it is the semiconductor material that is mostly used when it comes to vertexing and to tracking detectors in particle physics. But why is it exactly silicon, that is used as detector material in high energy physics?

Silicon is a semiconductor with a relatively small band gap (1.12 eV). An electron-hole pair can be created with very little energy (approximately 3.6 eV- compared to e.g. Argon gas 15 eV). This leads to a better energy resolution and a high signal- thus no gain is needed. Silicon is a very dense material, therefore the energy loss for silicon is higher than for other materials. That makes it possible to use thinner detectors, it reduces the quantity of secondary particles and also improves the spatial resolution. Silicon also has a high carrier mobility, which means that its charge carrier are fast- less than 30 ns are needed to collect the entire signal. For silicon there is a large experience in industry when it comes to micro-chip technology, that's why there are industrial fabrication techniques. Another plus factor of Si is its high intrinsic radiation hardness. It is because of all the listed advantages that silicon is the standard semiconductor material used in particle detectors.

3.5. Doping

Nevertheless usually it is not pure silicon that is used as detector material. In most of the applications a certain number of atoms in the lattice are replaced by atoms of the neighboring columns of the periodic table, a process that is called doping. A semiconductor can be doped either with atoms of a material that has one valence electron more or less than the material itself. Silicon, e.g. can be doped with a material of either 3 or 5 valence electrons. Let's imagine that silicon is doped with a material that has 5 bonding electrons (e.g. P, As, Sb), then there will be an atom in the lattice with 5 instead of 4 valence electrons, thus there will be one electron more that is available for conducting current. Such a doping process is called n-doping, where n stands for negative, since with the additional electron there is a surplus of negative charge carriers. The resulting material is called n-type semiconductor or donor. The same procedure can be done with an atom that has only 3 valence bondings. Doping the Si crystal with materials that have a valence of 3 (e.g. B, Al, Ga, In), results in an atom with a supplementary hole in the valence band or a so called p-doped silicon. P stands for positive because in this case there is one more positive hole that is available for conducting. Such a p-semiconductor is also called acceptor.

3.6. The p-n- junction

When it comes to the use of semiconductors in electronics one of the most important structures is the p-n junction. It is also very important for constructing particle detectors in high energy physics. A so called p-n junction is obtained by simply joining together a p- and an n-doped semiconductor. If used as an electrical component the p-n-junction is equally called diode. So what happens if you bring together two semiconductor of opposite doping? And what are the electrical properties of such a component? The answer can be seen at figure 3.1. Whereas p-doped and n-doped material is rather conductive (depending on the quantity of doping) p-n- junctions can be highly resistive (depending on the applied voltage). When p- and n-doped materials are brought together there is a so called space charge region (also called depletion zone) that evolves, because the free charge carriers (electrons for n-doped and holes for p-doped material) diffuse in the oppositely doped material. The free electrons of the n-side drift to the p-side and recombine with the holes, the holes of the p-side move to the n-side and recombine with the free electrons. Due to this diffusion the depletion zone is free of charge carriers. The electrical behavior of the p-n-junction now is strongly dependent on the sign of the externally applied voltage. If a negative voltage is applied to the n-doped material and a positive voltage to the p-side the electrons and holes are refilled to the depletion zone and the depletion zone becomes narrower. The diode is now switched in forward direction and is electroconductive. If however, a positive voltage is applied to the n-doped side and a negative voltage to the p-side, the electrons and holes are pulled out of the depletion zone. In this case the p-n- junction behaves like an insulator (the diode is switched in reverse direction) until the avalanche voltage (breakthrough) is reached. In semiconductor detectors p-n junctions are operated in reverse direction.

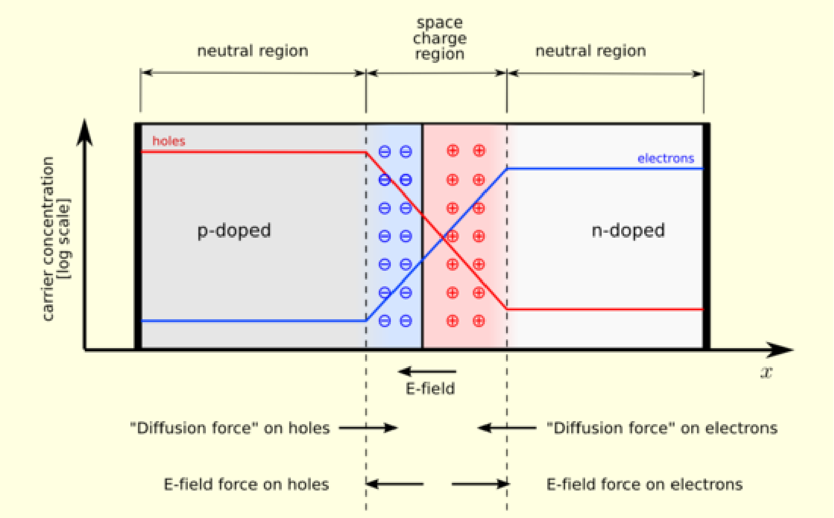

Figure 3.1.: p-n junction, depletion zone [8].

3.7. Strip detector basics

In principle a semiconductor particle detector is a modified p-n junction (see the former chapter) that is biased in reverse direction. So the negative voltage is applied to the p-side and the positive voltage to the n-side, resulting in a growth of the space charge region. To be sensitive to particles the sensor has to be fully depleted, which means that the space charge region (SCR) has to cover the full detector. The large-area diode is split into strips and each of the strips is read out by its own electronics. It consists of a p-n junction with a metalized n^+ layer on the bottom side, to avoid a Schottky contact and to improve the ohmic contact. Also, for a connection of each detector strip to the readout electronics an aluminum metalization is applied to all strips of p^+ implant. If now a charged particle goes through the fully depleted p-n- junction about 30.000 electron-hole pairs are created which due to the applied electric field move to the anode respectively the cathode - electrons drift towards the n^+-layer and holes towards the p^+ layer . An amplifier is linked to every strip that amplifies the signal. From the signals that are measured on the individual strips the position of the traversing particle can be deduced. There are n- and p-type detectors, the given one is of n-type (which means that the bulk is made of n-type silicon). There are a several reasons why most of the detectors are of n-type, including tradition and also the easier production process. Nevertheless p-type detectors have also some advantages, especially when it comes to high radiation (which isn't a big topic in the Belle II project though). Typical parameters for an n-type Silicon strip detector are a thickness of 300 μm, a strip pitch (distance between the strips) of about 50-200 μm, an operating voltage of lower than 200 V (100 V for the SVD) and an n- type bulk of $\rho > 2\text{k}\Omega\text{cm}$.

3.8. AC coupled strip detector

The strip detectors in the Belle II SVD are AC coupled strip detectors (see figure 3.2). In the AC coupling or capacitive coupling, there is no direct electrical contact between the aluminum strip and the p^+ layer, but in between there is a thin film of silicon oxide (100-200 nm). The resulting capacitances are between 8-32 pF/cm. The layers aluminum, SiO_2 and implant form an integrated capacitor that separates the readout circuit from the biasing circuit. So the advantage of AC coupling is that it blocks the leakage (DC) current from the amplifier. There can be so called pinholes, which are shortcuts through the dielectric. The strips with pinholes can be a problem for a sensor. If the radiation damage on the sensor increases they can lead to a higher leakage current and also a smaller signal. Since the film of SiO_2 cuts the bias connection through the strips, an alternative to connect it has to be found. In the case of the trapezoidal Micron sensors it is connected by poly silicon resistors (see the next section).

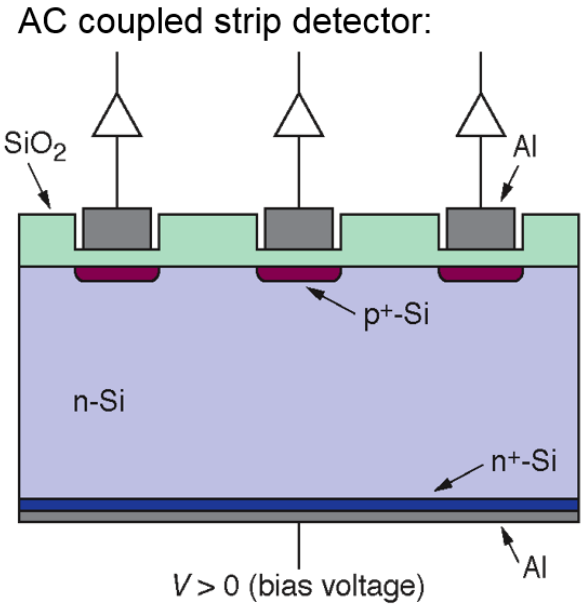

Figure 3.2.: Schematic view of an AC coupled silicon strip detector with traversing ionizing particle. [9]

3.8.1. Polycrystalline silicon bias resistor

Considering that a strip sensor usually consists of several hundred strips, it can be well understood that the bias voltage cannot be applied to each strip separately. Therefore each strip implant is connected to a so called bias line via bias resistors. The bias voltage is then only applied to the bias line but via the bias resistors it is also connected to each implant (see the schematic on figure 3.3). Usually the bias resistor is made out of polycrystalline silicon, that's why it is also called poly resistor. To keep the noise as low as possible normally very high resistances (in the order of MΩ) are chosen. Nevertheless the resistance is limited by the production process and also the voltage drop across the bias resistor during the operation.

3.9. Double Sided Silicon Detectors (DSSD)

An advanced sensor architecture that is used in the Belle II SVD is the Double Sided Silicon Detector (DSSD, see figure 3.4). DSSDs are two-sided types of AC coupled strip detectors. For those sensors the strips are arranged orthogonally on both detector sides. DSSDs are practical because they enable a more elegant way of measuring two coordinates and- since one sided detectors can only resolute one coordinate- their use saves material when a two dimensional read out is desired. A minimal material budget is crucial in the Belle II project to minimize multiple scattering. The difference to the AC coupled detector discussed in the previous chapter is that now there are also strips, namely n$^+$-strips with AC coupled aluminum metalization on the backside of the sensor.

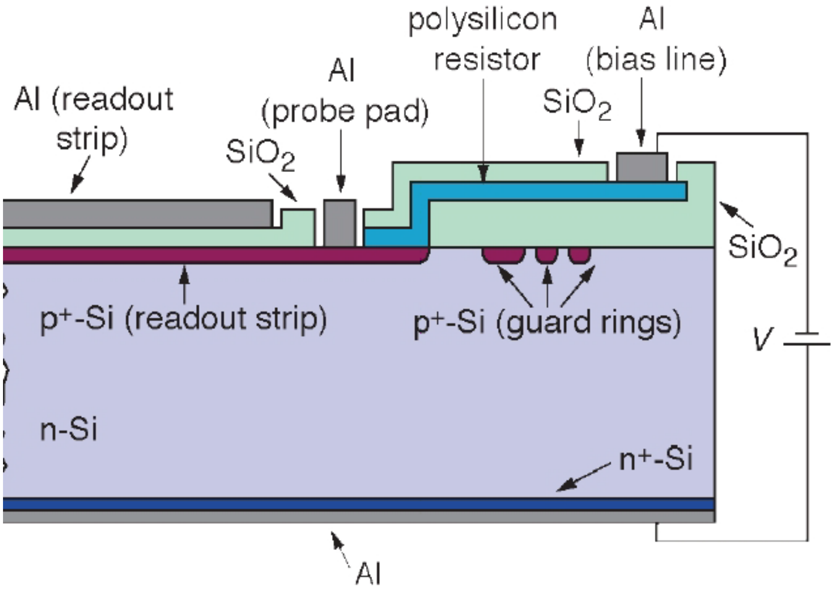

Figure 3.3.: AC coupled strip detector with integrated poly resistor.[9]

Those are orthogonal to the p^+ strips on the other side. The side with the n^+-strips is called n-side, the one with the p^+ strips is called p-side. In the case of the trapezoidal Micron DSSDs the p-sides of the sensors include 768 long strips with a strip pitch of 50-75 μm between the strips that measure the $R\Phi$ -coordinate. The n-sides include 512 shorter strips with a strip pitch of 240 μm that are allocated perpendicular to the p-side strips. Between each two read out n-side strips there is one intermediate strips that isn't read out but that improves nevertheless the resolution (see section 3.9.3). The n-side strips measure the z-coordinate. The number of strips per side is a multiple of 128, because this is the number of input channels of the readout chips. Again, to successfully operate a DSSD the SCR has to reach the borders of the device, respectively the sensor has to be fully depleted. If a particle goes through such a fully depleted DSSD- again about 30.000 electron-hole pairs are created, and in this case the holes drift to the p^+ strips, whereas the electrons drift to the n^+ strips, so that by reading them out simultaneously the point where the particle entered the detector can be determined. This is how a very fine resolution (in the order of micrometers) can be achieved.

3.9.1. Advantages and disadvantages

There are several advantages of a DSSD, like a save in material budget and that they are a more elegant way to measure two coordinates. The disadvantages are the very complicated manufacturing and handling procedures, which also make them expensive- one sensor costs several thousand Euros. Moreover they need a special strip insulation of the n-side (p-stop, p-spray techniques) to avoid the building of an accumulation layer (see next section). Also, they show ghost hits at high occupancy (see figure 3.5). If two hits come in at the same time, at first it cannot be known at which cross sections of the

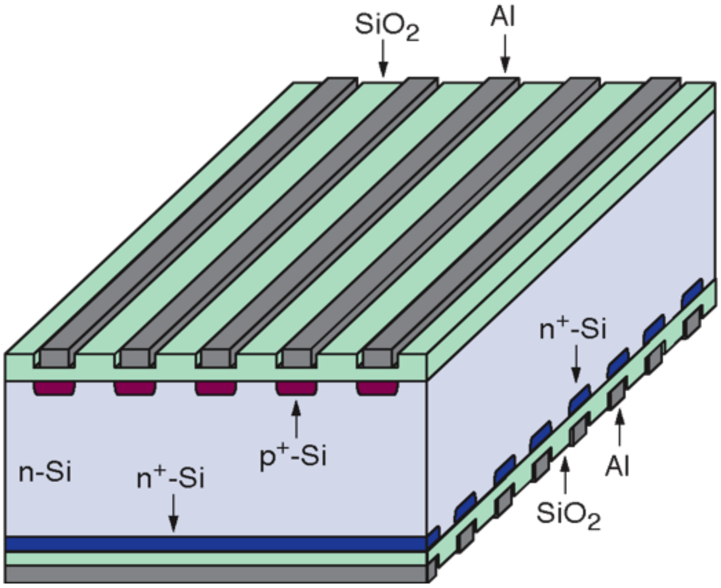

Figure 3.4.: Double Sided Silicon Detector. [9]

strips are the real and on which one the ghost hits appear. Nevertheless, the track of the real particle can be reconstructed with data from other detector layers.

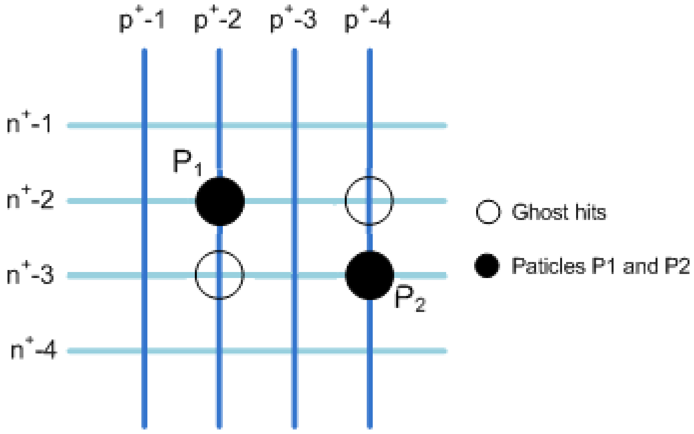

Figure 3.5.: An example for the creation of ghost hits. There are four possible positions for two particles traversing at the same time.

3.9.2. Accumulation layer, p-stop and p-spray technology

There is one problem needed to be solved in the handling of DSSDs. On the n-side there are static, positive oxide charges in the interface between silicon and silicon oxide, which attract electrons. So there is an accumulation layer developing beyond the silicon oxide and thus the n^+-strips are no longer isolated from each other but have a finite resistance (see figure 3.6). This process destroys the whole position resolution on the n-side. There are a several techniques (e.g. p-spray, p-stop, field plates) to solve this problem, the one Micron used on the trapezoidal Belle II sensors is the p-stop technology. In the p^+ implant (p^+ stop) technology, there are extra p^+ implants added (see in figure 3.7 (a)) between the n^+-strips. They disrupt the electron accumulation layer and an inter-strip resistance of several GΩ is obtained.

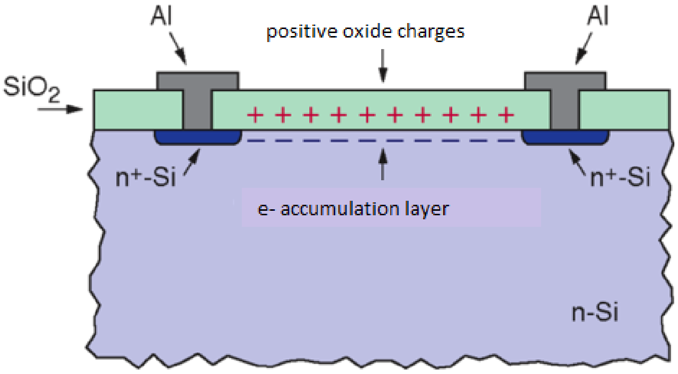

Figure 3.6.: Problem of n^+-segmentation, positive oxide charges cause electron accumulation layer. [9]

Another solution to the problem of the accumulation layer built is the p-spray technology. Using the p-spray technology, the whole surface of the n-side is slightly p-doped which also breaks the electron accumulation layer (see in figure 3.7 (b)).

3.9.3. Intermediate strips

The resolution of the strip sensors is largely dependent on the strip pitch. The smaller the strip pitch the better the resolution that can be reached. Nevertheless a small pitch distance also leads to a higher number of electronic channels, which results in higher

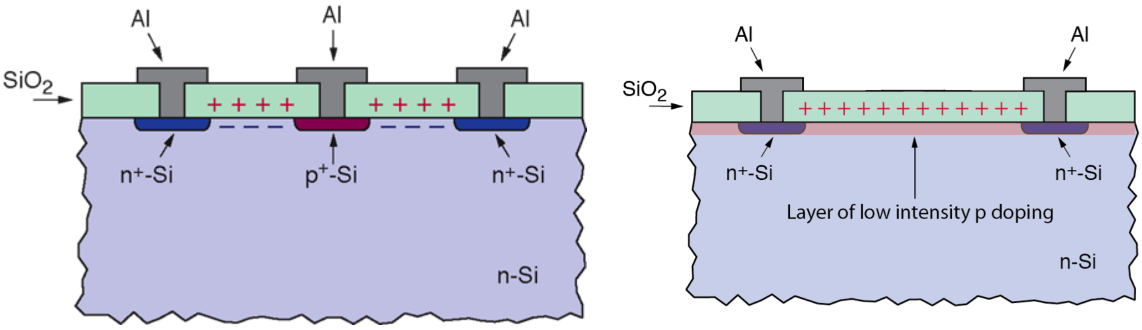

(a) Schematic of a p^+-stop structure. [9]
(b) Schematic view of the p^+-spray technology. [9]

Figure 3.7.: Schematic and implementation of intermediate strips.

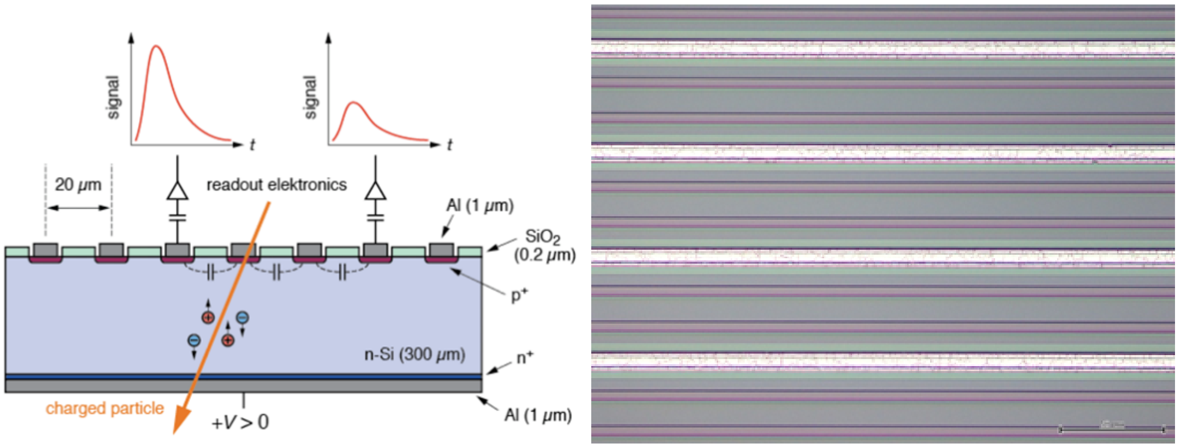

(a) Schematic of a detector with two intermediate strips. [9]

(b) Intermediate strips on a Belle II Micron sensor

Figure 3.8.: Schematic and implementation of intermediate strips.

costs and higher power consumption (and also a stronger cooling needed). So there is a clever method to increase the resolution by keeping the costs almost unchanged. It is the implementation of intermediate strips [10] that are not connected to the read out electronics. It is then by capacitive coupling that the signal of those strips is transferred to the readout strips. This leads to a higher resolution. The principle with two intermediate strips can be seen schematically (for a DC detector) on figure 3.8 (a) and the implementation on the Belle II SVDs can be seen on figure 3.8 (b).

3.9.4. Passivation layer, AC and DC pads

As protection from mechanical damages, such as scratches or from interaction with air moisture, the uppermost layer of the DSSDs is a 1 μm-thick SiO$_2$ film. At certain areas of the sensor surface the passivation is etched to provide an electrical contact, for example at certain areas of the bias ring (to contact the bias voltage) and the strips (DC pads). There are two kind of pads (see figure 3.9) and they are around twice as large as the strip width, to facilitate contacting them with the probe needles.

- **AC pads**: AC pads are crucial for detector operation. They are broader parts of the readout metal layer. The readout chip is wire bonded to the AC pad area. Also some quality management measurements use AC pads.
- **DC pads**: DC pads are electrically connected to the implant. They are very important for the quality assurance process of the sensors.

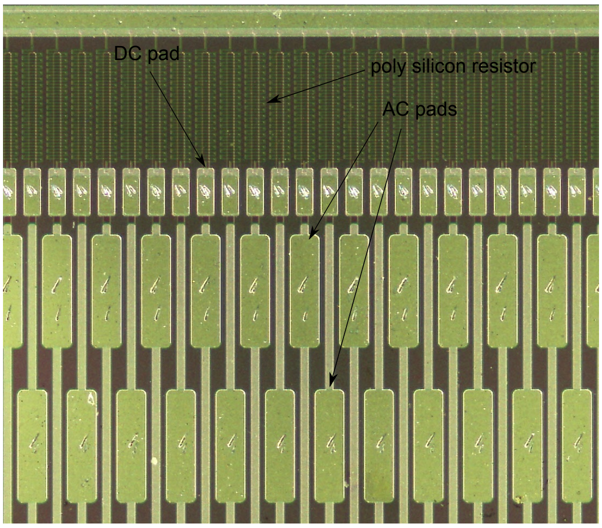

Figure 3.9.: DC pads, AC pads and poly silicon resistor.

4. Statistical methods

In section 6 a number of different statistical methods is used to analyze the measurement results. The given chapter will introduce the basics of the methods used.

4.1. Histogram

A histogram is a graphical display that gives information about the distribution of the measured samples. An example for a histogram can be seen on figure 6.4. The given histogram shows the distribution of the single strip current of the n-side and the sensors measured in Vienna. To make a histogram the first step is to group the whole range of values in bins and then look how many of the values fall into each interval. After that a rectangle is drawn with the height proportional to the counts and the width equal to the bin size, in the given example the width is 1 nA.

4.2. Normal distribution

The normal distribution is a probability distribution that is valid in many fields of science. It is also called Gaussian distribution, because it was discovered by Carl Friedrich Gauss. Many values follow a normal distribution. This is because of the central limit theorem, which says that if an event is the sum of a large number of other random events it will be normally distributed. Also the variables measured in the sensor tests (see section 6) should follow normal distributions. Figure 4.1 (a) shows a Gauss fitted histogram. The most important parameters in a Gauss curve is the mean value and the standard deviation. The mean value is the value at the peak of the distribution, ± the standard deviation gives the width of the distribution. Also in the interval with a deviation of $\pm\sigma$ there are 68.2% of the results. On the given plot both the standard deviation (here: σ) and the mean value (μ) is variated. The associated formula to the Gauss function is formula 4.1.

$$f(x,\mu,\sigma) = \frac{1}{\sigma\sqrt{2\pi}} e^{-\frac{(x-\mu)^2}{2\sigma^2}} \tag{4.1}$$

4.3. Skewness

In statistics the skewness is a measure of the asymmetry of the probability distribution. The skewness is the central moment of 3rd order- its formula can be seen in equation 4.2. The skewness can be positive, negative or zero. Since a Gauss curve is perfectly symmetrical, its skewness is zero. In case of a negative skew, the left tail is longer and the mean of the distribution is concentrated on the right of the figure. If there is a positive skew the right tail is longer and the mean of the distribution is concentrated on the left side of the figure. Figure 4.1 (b) shows examples of distributions with negative respectively positive skewness.

$$v = \frac{1}{n}\sum_{i=1}^{n}\left(\frac{x_i - \bar{x}}{s}\right)^3 \tag{4.2}$$

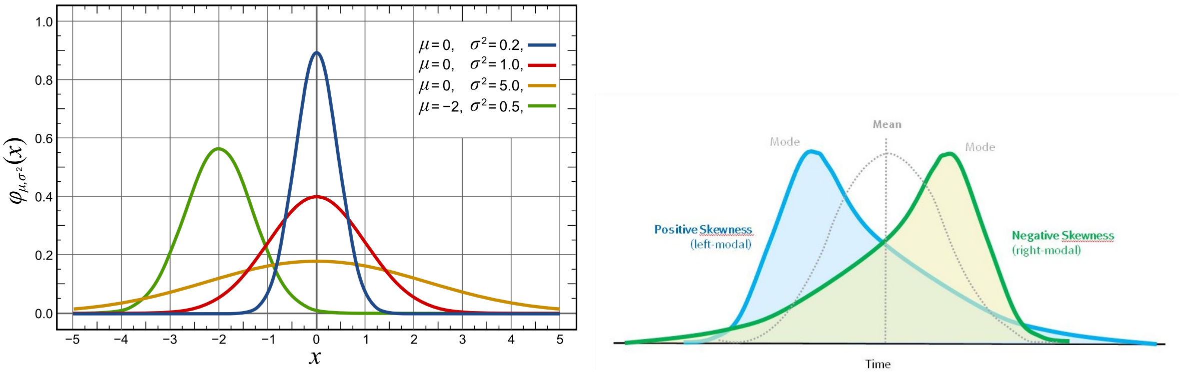

(a) Normal distribution with different means and standard deviations.[11]

(b) Positive and negative skewness.

Figure 4.1.: Normal distribution, mean, standard deviation and skewness.

4.4. Kurtosis

In statistics kurtosis is a measure of the "peakedness" of a probability distribution. Similar to the concept of the skewness, it is a descriptor of the shape of a distribution. The kurtosis is the central moment of 4th order (see formula 4.3). Distributions with little kurtosis scatter rather uniformly while for those with a high kurtosis the scattering results rather from extreme, rare events. To better estimate the kurtosis of a distribution it is compared to the kurtosis of the normal distribution, which is β=3. To enable better comparison a new variable is introduced, the so called excess γ- which is $\gamma = \beta - 3$. Now distributions with an excess of zero are called mesokurtic- they have the same kurtosis than the normal distribution. If the excess is higher than 0, the distribution is called leptokurtic- in this case the distribution is pointier than the Gauss distribution. And finally, if the excess is negative the distribution is called platykurtic - in this case the distribution is flatter than the Gauss distribution (see on figure 4.2).

$$w = \frac{1}{n}\sum_{i=1}^{n}\left(\frac{x_i - \bar{x}}{s}\right)^4 \tag{4.3}$$

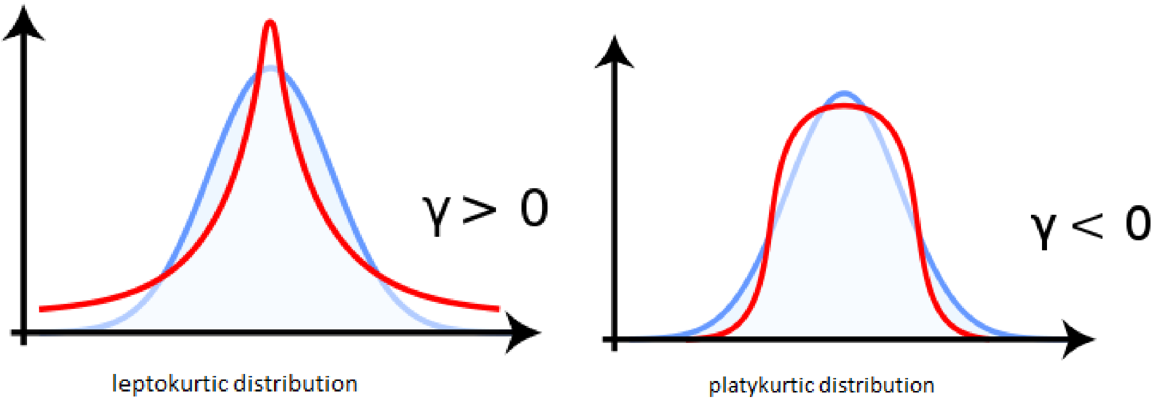

(a) Distribution with positive kurtosis.

(b) Distribution with negative kurtosis.

Figure 4.2.: Negative and positive kurtosis.[12]

4.5. Box plot

A box plot is a diagram to graphically depict a data distribution. In our case it shows mean, median, the upper and the lower quartile, the minimum and the maximum of a given distribution. By looking at the box plot it can be seen for example if a certain distribution is symmetrical and if it has a lot of outliers. Figure 6.8 shows the box plot of the single strip current measurements of the n-side in Trieste. As explained on the plot there is a lot of different information one can get by analyzing the box plot. The maximum and the minimum value of the given sensors can be seen as crosses, the mean value is illustrated by a square and the median is the line in the box. The box shows the so-called interquartile range (IQR), the lower part shows the lower quartile and so 25-50% of the data (which means that 25% of the values are smaller than the data) and the upper part of the box the upper quartile, so 50-75% (in this case, 25% are larger than the data) of the data. The whiskers show the range between the 10th percentile and the 90th percentile, so 80% of the data is in the range of the whiskers.

4.6. Correlation coefficient

A correlation depicts the relation between two or more variables, events or functions. There doesn't have to be a causal relation between the two variables. In statistics the relation between two variables is for example measured with the correlation coefficient of Bravais-Pearson. This correlation coefficient is obtained by dividing the covariance of the two variables by the product of their standard deviation, see formula 4.4. In the given formula $\bar{x}$ respectively $\bar{y}$ are the mean values of the variables x and y. n is the quantity of measurements and s_x respectively s_y are the standard deviations of the variables. The correlation coefficient is only defined if the standard deviations are finite and nonzero. The range of the coefficient is between +1 and -1. The Pearson correlation is +1 in the case of a perfect linear relationship (correlation) between the variables and -1 in the case of a perfect decreasing linear relationship (anticorrelation). So it indicates the degree of linear dependence between two variables. If the variables are completely independent the correlation coefficient is zero.

$$r = \frac{1}{n-1} \sum^{i} \frac{(x_i - \bar{x})(y_i - \bar{y})}{s_x s_y} \tag{4.4}$$

4.7. Linear regression

Linear regression is a special case of regression analysis which tries to explain the relationship between a dependent variable and one or more independent variables. It tries to predict a certain variable by another variable and assumes a linear relation. Formula 4.5 shows the formula for linear regression. It is reasonable to calculate a linear regression if there is a strong correlation or anti-correlation found between two variables. In the case of the sensors the single strip current should be positively correlated with the total leakage current of a sensor.

$$y = a + bx \tag{4.5}$$

4.8. Two-sample t-test, Welch's t-test

The student's t-test is a hypothesis test in mathematical statistics. The t-test for two means tests if the two population means differ from each other. There are the following conditions for the t-test for two random samples:

- The two populations are independent (their results don't affect each other).
- The answer variable (y) is a quantitative variable (its values are counts or measurements).
- The y-values for both populations are nearly normally distributed (the means can differ).

If the two variances of the normal distributions differ from each other (the two sample sizes may or may not be equal) the Welch's t-test has to be used. In testing the so-called null hypothesis that the difference of the population mean is equal to zero, one uses the t statistic which is calculated as:

$$t = \frac{\bar{X}_1 - \bar{X}_2}{\sqrt{\frac{s_1^2}{n_1} + \frac{s_2^2}{n_2}}} \tag{4.6}$$

with $\bar{X}_i$ being the sample means, s_i^2 being the sample variances and n_i being the sample sizes.

The value of the degrees of freedom d.f. that are linked to the variance estimate is approached with the Welch-Satterthwaite equation:

$$d.f. = \frac{(\frac{s_1^2}{n_1} + \frac{s_2^2}{n_2})^2}{\frac{s_1^4}{N_1^2 n_1 - 1} + \frac{s_2^4}{N_2^2 n_2 - 1}} \tag{4.7}$$

After the t and d.f. is calculated, the t-value is compared with a t-distribution with the appropriate number of degrees of freedom d.f. to obtain the p-value that then IS or IS NOT sufficient to reject the null hypothesis. For example, if the p-value is lower than 0.05 the two population means differ at a significance level of 5%.

5. Electrical Characterization Setup for DSSD

Quality control is a very important point when it comes to silicon strip detectors. Before they are mounted onto the ladders, the silicon sensors have to be tested rigorously and it has to be made sure that certain requirements are fulfilled to ensure their functioning in the experiment. A characterization of the devices is done electrically (by measuring currents, resistances and capacitances), mechanically (measuring the geometrical dimensions) and optically (dust, dirt, scratches, issues with the lithography). Since the DSSDs are very expensive they have to fulfill very strict specifications. Acceptance criteria are defined (number of non-working strips under a defined percentage) and the non-working strips have to be excluded from being used. Non-working strips are for example strips with pinholes (described later in this section).

5.1. The QTC Vienna

The typical setup at HEPHY Vienna to check the electrical parameters of the sensors is the Quality Testing Center (QTC). It consists of a light-tight box (see figure 5.1), measuring instruments and a computer running NI Labview. It is a full scale automated setup, designed for electrical measurements on silicon strip sensors. There is a motorized XYZ-table that can be operated either manually using a joy stick or automatically by the computer. It can move the sensor very precisely up to the micron scale. Also there is a vacuum support to fix the sensor at the table. There are two positioners on the right that are mounted onto the XYZ-table and that contact the bias voltage during the measurement. On the left side there are three positioners, two DC needles and one AC needle to contact the sensor for the strip scan measurements. They contact to the AC and the DC pads of the measured sensor. To start, before each measurement there is an alignment procedure that has to be done. This is due to the different geometries of every sensor. First the LabView program reads in the so-called pad file, that contains the information about strip number and position of the given sensor. In the alignment the table moves to the first pad. If it doesn't move to the right place, the position can be adjusted manually with the joystick. Then the table moves to the last strip. Again the position can be adjusted manually. After the alignment the needles are contacted and the measurement can be started. Now the table can go automatically from one strip to the next and measure the important strip parameters (I_{strip}, R_{poly}, C_{ac} and I_{diel}, see section 5.2.2). Also single strips can be measured using the single strip measurement.

To avoid scratching of the sensor the z-axis lifts while going from one to the next strip.

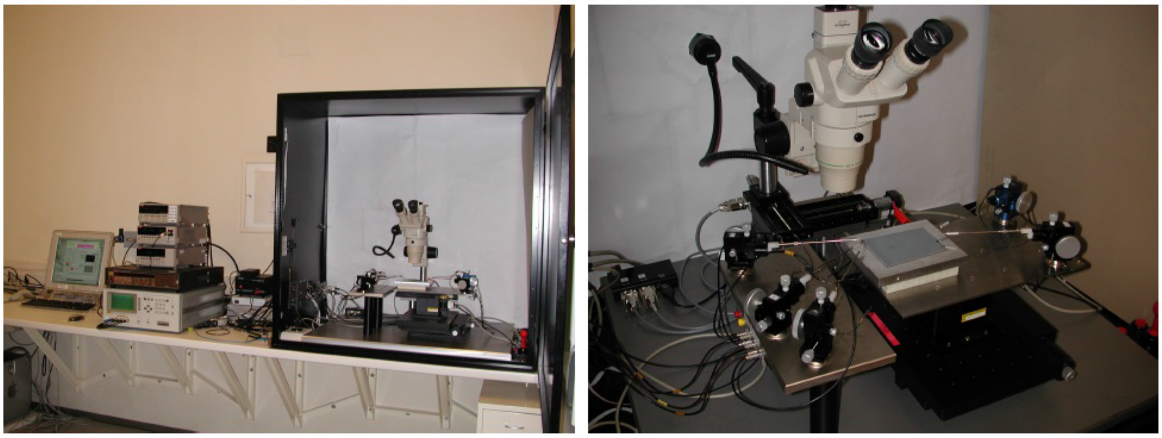

Figure 5.1.: Left: the computer, the measurement instruments and the light-tight box. Right: Zoom in the light-tight box: the XYZ-table, the positioners, the microscope and the light source.[13]

The instruments used for the measurements can be seen in figure 5.2. They are operated automatically by the LabView software. The electrical measurements at HEPHY are done with:

- A **Keithley 6514 electrometer**
- An **Agilent 4284A LCR meter**: A LCR meter is an instrument that can measure inductance (L), capacitance (C) and resistance (R) of a component.
- A **primary source measure unit (SMU)**: The source measure unit (**Keithley 237**) has a voltage source, a constant current source, an Amp- and a Voltmeter -all in one device. It has a high precision Ampmeter (250fA at 700V) and needs therefore Triax connectors to enable high precision measurements.
- A **Keithley 2410 secondary source measure unit (SMU2)**
- A **Keithley 7001 switching matrix frame** that is equipped with two 7153 matrix cards (with 5x4 contacts).
- The **THRX system**, that is used to monitor temperature and humidity in the light-tight box.
- A **microscope**, that enables a more accurate contacting of the needles to the sensor pads.
- A **light source** illuminating the sensor for better contacting.

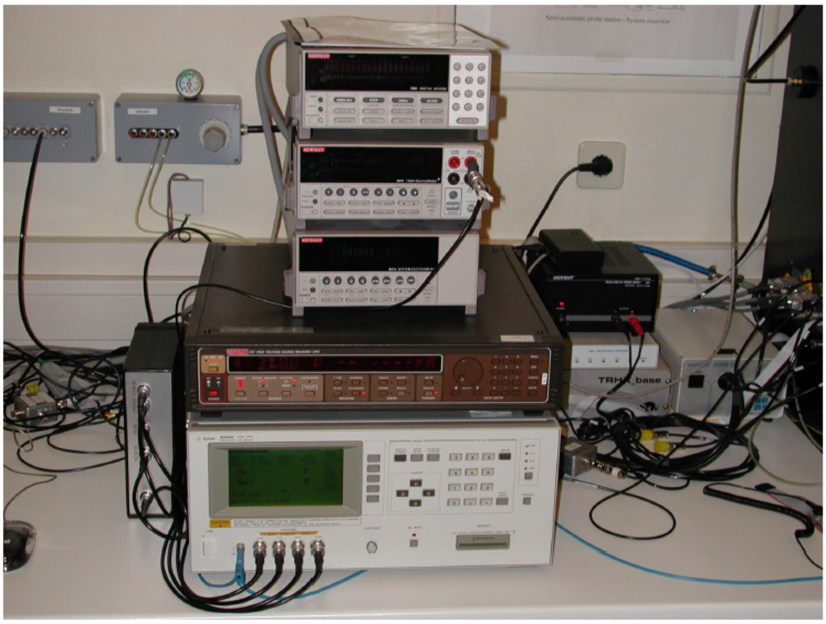

Figure 5.2.: The instruments for the electrical measurements at the QTC Vienna.

We test electrical parameters and strip failures of the detectors. Common strip failures are open strips (see figure 5.3 (a)) , shorted strips (figure 5.3 (b)), open bias resistors (figure 5.3 (c)), open implants (figure 5.3 (d)) and pinholes (shorts between the implant and the metal, figure 5.3 (e)).

Besides the QTC there are supplementary measurements that can be also performed on the sensors: There is also a coordinate measurement machine (CMM) at HEPHY that can be used to measure the mechanical parameters. It is a 3D mechanical measurement system to determine the sag, bow and thickness of the sensors. Moreover other optical measurements on the sensors can be done on site in the cleanroom of the HEPHY using a second microscope with higher magnification or using transmission electron microscopy or scanning electron microscopy at the USTEM [1] at the Vienna UT.

5.2. Measurement types

Each type of measurement requires its own configuration of probe needles and instruments, so its own matrix configuration. The schematic functioning of the switching matrix is shown in figure 5.5. There are two two-dimensional switching matrices, so three indexes are required to determine a specific configuration. The first index refers to the matrix, the second to the line and the third to the column of the matrix. For example (1,1,1) means that on the first matrix the first contact is closed- so, SMU low is connected to the bias line by one of the bias needles.

---

[1] Universitäre Service-Einrichtung für Transmissionselektronenmikroskopie.

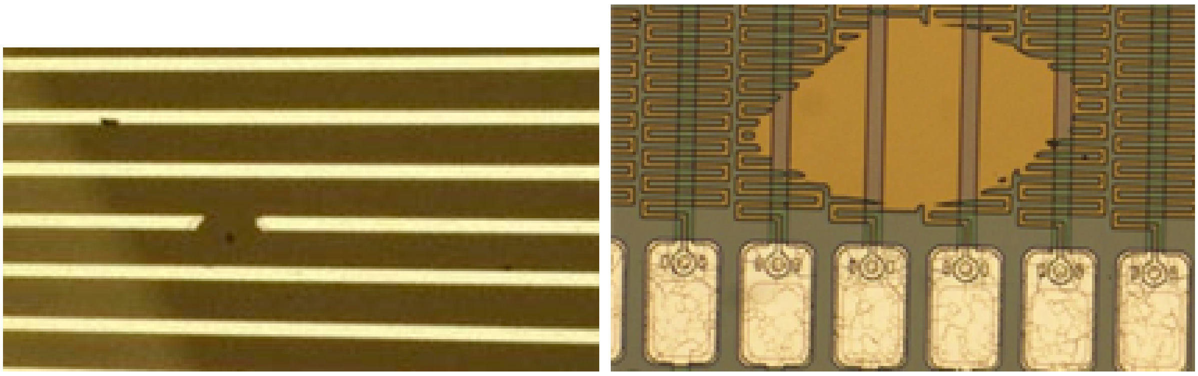

(a) Open strip.

(b) Open bias resistor.

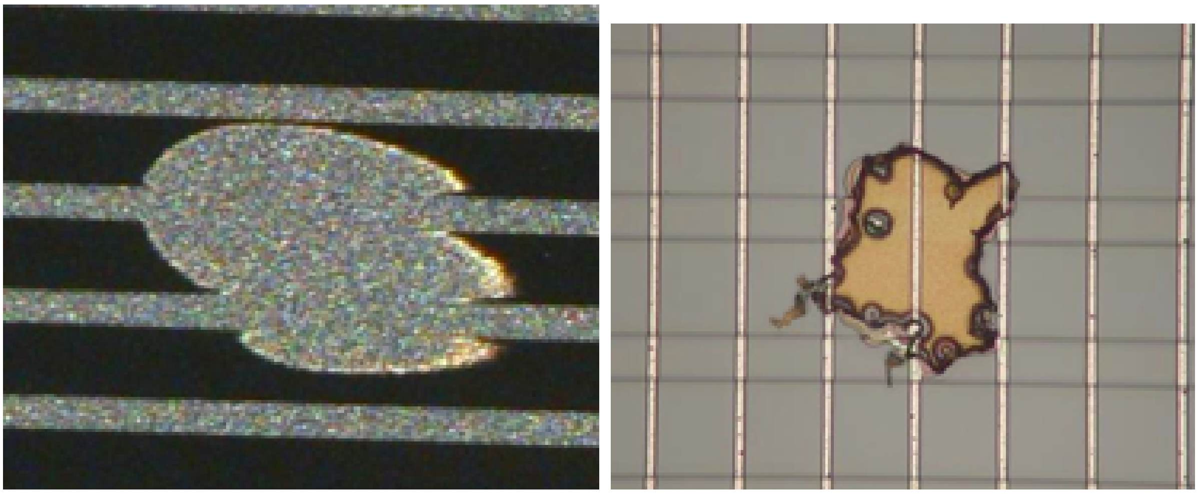

(c) Shorted strip.

(d) Open implant.

Figure 5.3.: Common strip failures.

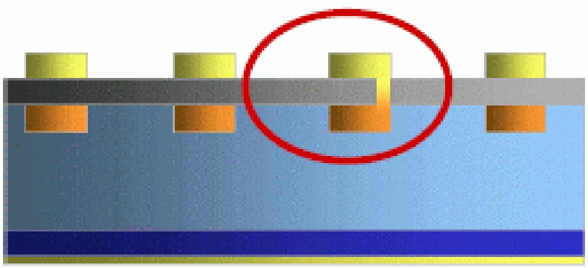

Figure 5.4.: Pinhole (short between implant and metal).

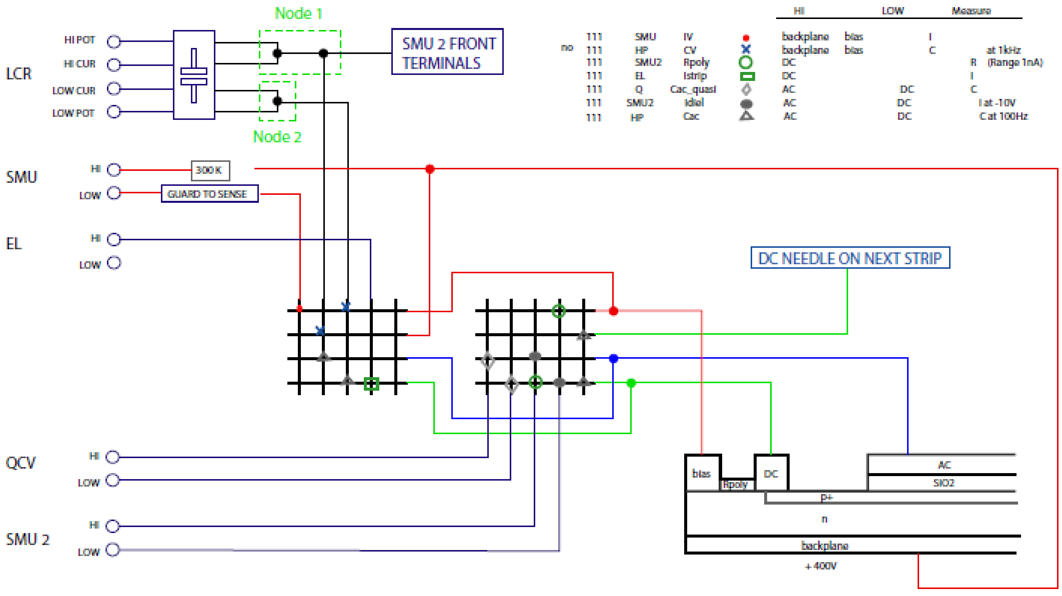

Figure 5.5.: Schematic functioning of the switching matrix.

5.2.1. Global scans

5.2.1.1. Global IV curve

There are two global curves that are usually tested, one is the IV curve. It is needed to determine the dark current I_{dark} (see later in this chapter) and also the breakthrough voltage. The reverse bias voltage is ramped up (normally in steps of 5 V) from 0 V until 200 V and the total leakage current of the sensor is measured. To measure an IV curve the needed matrix configuration is (1,1,1). The low output of the SMU is connected to the bias line and the high output to the backplane. High voltage is always applied to the backplane while the bias line is grounded. An IV curve can be seen on figure 5.6.

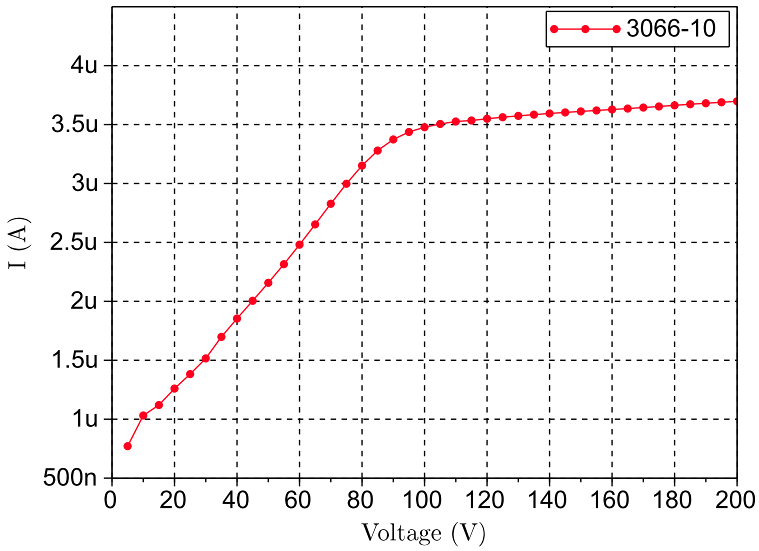

Figure 5.6.: IV curve measured for the Micron sensor 3066-10.

5.2.1.2. Global CV curve

The other global curve is the CV curve to determine the depletion voltage and the total capacitance. It is also measured by ramping up the bias voltage in steps of 5 V from 0 V to 150 V, so again the (1,1,1) connection is closed. After the voltage is applied the LCR measures the capacitance of the sensor bulk by closing channels (1,2,2) and (1,1,3). Now both the low terminal of the LCR meter and the SMU are connected to the bias line, therefore the low terminal of the SMU has to be disconnected for the measurement to prevent a short between the LCR meter and the SMU. With increasing bias voltage the total capacitance decreases, the bulk material is depleted from charge carriers until the bulk material is fully depleted. When the $1/C^2$- curve is plotted, the depletion voltage can be spotted at the bend of the graph, figure 5.7 shows that curve. By fitting the function with two straight lines from the left and the right, the depletion voltage was determined.

5.2.1.3. Dark current I_{dark}

The dark current I_{dark} of the whole sensor is an important global parameter. It is measured at the operating voltage of the SVD which is at 100 V. The dark current of the sensor should be as low as possible, to have as little noise as possible that disturbs the measurement.

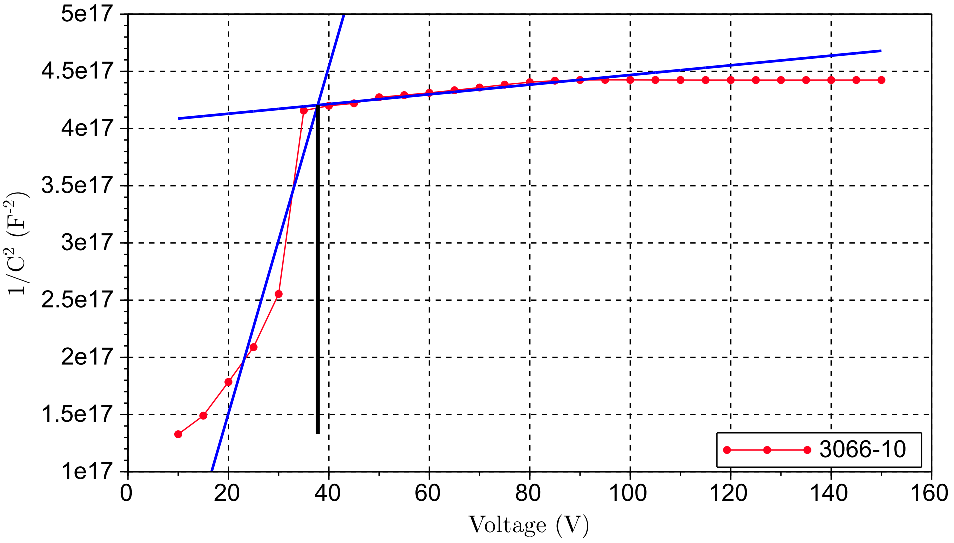

Figure 5.7.: $1/C^2$- curve measured for the Micron sensor 3066-10. The two fitted straight lines (blue) intersect at the depletion voltage (here: approximately 38 V).

5.2.2. Measurements on strips

To gain more precise information about the quality of silicon sensors, strip scans were performed. This setup tests the electrical properties of every strip individually. During all of the strip measurements the sensor is over-depleted, which means that the bias needles of the two positioners are contacted on the bias lines on p- and n-side. The bias voltage is applied before the measurement starts until the strip scan is finished. So all the time during the measurements the contact (1,1,1) of the switching matrix has to be closed. The probe needles are connected to the AC and DC pad and the XYZ-table moves automatically from one strip to the next, scanning all strips of the sensors. The result of a typical strip scan can be seen on figure 5.8. There are four important strip parameters that are measured.

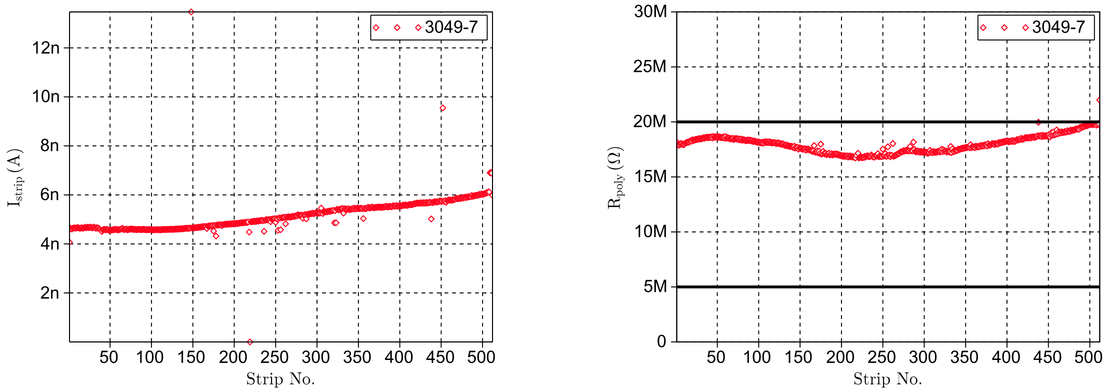

(a) Single strip current of sensor 3049-7 (n-side).

(b) Poly resistor of sensor 3049-7 (n-side).

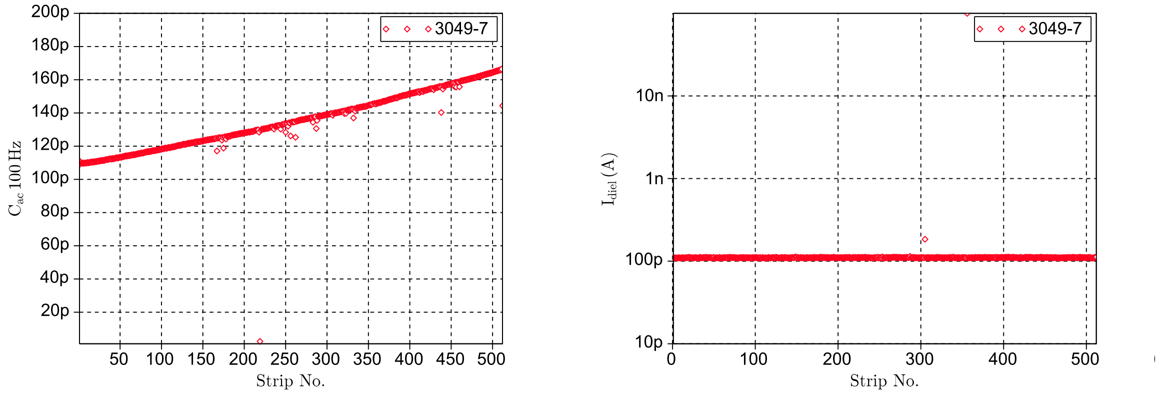

(c) Coupling capacitance of sensor 3049-7 (n-side).

(d) Dieletric current sensor 3049-7 (n-side).

Figure 5.8.: Complete strip scan of Micron sensor 3049-7 with all 4 important parameters

5.2.2.1. Single strip leakage current I_{strip}

One of them is the strip leakage current I_{strip}, which is the dark current of the implants. It is measured for the signal-to-noise ratio which suffers from noisy strips. Thus the strip leakage current should be as low as possible. Also a homogeneous strip leakage current is a quality feature for strip sensors. For measuring the single strip current, the needle on the DC pad has to be connected to the Keithley 6514 electrometer. That means that the contact (1,4,4) has to be closed. By doing that the bias resistors are bypassed and the single strip current can flow directly in the electrometer. Typical single strip currents are of some 100 pA to 10 nA.

5.2.2.2. Poly resistor R_{poly}

To measure the poly (crystalline silicon bias) resistors the SMU2 is connected via the switching matrix between the bias line and the DC pad. So the connections (2,4,3) and

(2,1,4) have to be closed by the switching system. The resistance is measured by the SMU2 in Ohms mode, which uses the SMU as current source and measures the voltage drop. The poly resistance is corrected using the single strip current that is measured before, because high single strip currents would change the resistance measurement, since the single strip leakage current has to flow through the bias resistors as well. Double sided strip sensors have poly-silicon resistances in the order of MΩ.

5.2.2.3. Coupling capacitance C_{ac}

The coupling capacitance C_{ac} is the capacitance between the aluminium layer and the p^+ implant across the SiO_2 dielectric. It is measured by connecting the LCR-meter between DC and AC pads. The connections (1,2,2) and (1,3,4) of the switching system have to be closed. So the AC needle that is on the AC pad is contacted to the high terminal of the LCR-meter and the DC needle that is on the DC pad and connected to the p^+ implant is contacted to the low terminal. If the implant or the metalization is interrupted, this will lead to a smaller capacitance, because then the disconnected area is no longer sensitive to the measurement. The coupling capacitance measurement can also be used to determine the thickness of the dieletric. The measurement works similarly to the measurement of the global capacitance, besides that only 100Hz frequency is used. If there is a short circuit between two neighboring strips the C_{ac} is twice the value of normal channels, so resistive pinholes can also be seen by the value of C_{ac} .

5.2.2.4. Dielectric current I_{diel}

The last important parameter is the dielectric current I_{diel}. It is the current flowing through the dielectric if 10 V are applied between implant and metal strip. It is the worst damage a single strip can have if there is a so-called pinhole, a short between the aluminum readout strip and the implanted strip. To measure the dielectric current the low terminal of the SMU2 is connected to the bias line, while the high terminal is connected to the AC pad. The configuration used is (2,3,3) and (2,4,4). This allows the SMU2 to apply a voltage between the metal layer and the implant, while measuring current. On a normal, functioning strip the current is between 100-200 pA. Pinholes can be easily detected when the SMU2 is driven into compliance (100 nA).

5.3. Specifications

5.3.1. Mechanical specifications

At the beginning of the Belle II project, Micron Semiconductors and HEPHY specified mechanical specifications for the trapezoidal double sided strip sensors. The thickness of the sensors had to be in the range of 300 μm ± 10 μm. It was the topic of a colleague's project work to determine the thicknesses of the sensors by using three different techniques (weighting, micrometer screw and electron microscopy). In total thirteen of the sensors that were shipped to Vienna for quality management didn't fulfill the strict width specifications. Since it doesn't make a big difference for the functioning of the sensors the specifications were changed to a thickness of 300 μm ± 20 μm. Then only three sensors were outside the specifications. For more information about the different methods used to determine the width of the sensors and also the results see [14].

5.3.2. Optical specifications

Optical quality control was done by means of the microscope to control the condition of the sensors before and after the measurements. The quality control with the microscope showed that our measurement procedures did partly damage the surface of the sensors. Figures 5.9 (a) and (b) show several examples of scratches found on measured sensors. There were different reasons for the damaging. One of them was a problem we temporarily had with the XYZ-table. For some time the table didn't move in z-direction which resulted in scratches on the sensors that were tested. Then, for several sensors the alignment process had to be repeated which resulted in contacting multiple times to the first pads which damaged the aluminum metalization on those strips (see e.g. figure 5.9 (b)). Also the surface of the aluminum metalization turned out to be very soft in comparison to the Hamamatsu sensors, so that even soft contacting with the probe needles resulted in scratches.

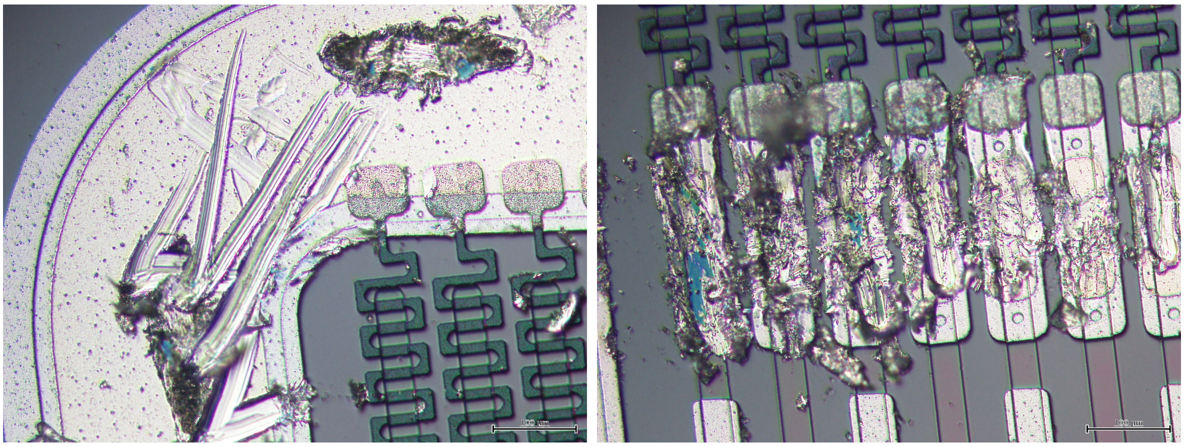

(a) Scratches on the surface of sensor 3048-2.

(b) First strips of sensor 3048-2.

Figure 5.9.: Optical quality control of sensor 3048-2

5.3.3. Electrical specifications

There are also a number of electrical specifications the sensors had to fulfill. Before the production process those requirements were determined by HEPHY and Micron Semiconductors (see the most important specifications arranged on figure 5.10).

- The dark current I_{dark} of the whole sensor had to be below 10 μA to keep the noise low. All sensors which exceeded the given value were rejected.

- The strip current I_{strip} had to be between 500 pA and 20 nA. A high strip current induces a high noise in the channel and makes it useless for particle detection.
- The original specifications for R_{poly} were between 10 and 20 MΩ. Our measurements showed that a lot of sensors didn't fulfill the strict requirements that were agreed to by HEPHY and Micron. The measured poly resistances varied between 5 and 50 MΩ. The difference of until 30 MΩ of the poly resistances of the former specifications aren't a big problem for the operation of the detector. That can be easily shown by estimating the voltage drop due to a high (e.g. 50 MΩ) poly resistance. Even assuming a very high strip current of 50 nA, according to Ohm's law ($U = RI$) the voltage drop on such a poly resistance would be of only 2.5 V. Comparing the operating voltage of 100 V and the measured depletion voltages of 20 to approx. 50 V a voltage drop of 2.5 V does by far not influence the correct functioning of the sensor. Therefore new limits were determined: The measured R_{poly} values of a given sensor should be in the range of the mean value of a sensor ± 5MΩ.
- The original specifications for the coupling capacitance C_{ac} were >1.2 pF per cm strip length and per strip width. This normed form was obtained by dividing the measured values through the length and the width of the strips. Most of the strips tested were outside these specifications. Since this was no big deal for the functioning of the sensors we also changed the specifications for the coupling capacitance. The new specification for good strips was that they had to be in the border of the mean value ± 20%.
- The dielectrical current I_{diel} had to be lower than 90 nA. If there was a pinhole at a given strip the SMU2 was driven into compliance (100 nA). If there were more than 0.5% pinholes on the sensors (so 3 for the n-side and 4 for the p-side) the sensor would have normally been rejected. But due to time restrictions of the Belle II project, sensors that had until 1% of pinholes were still accepted.

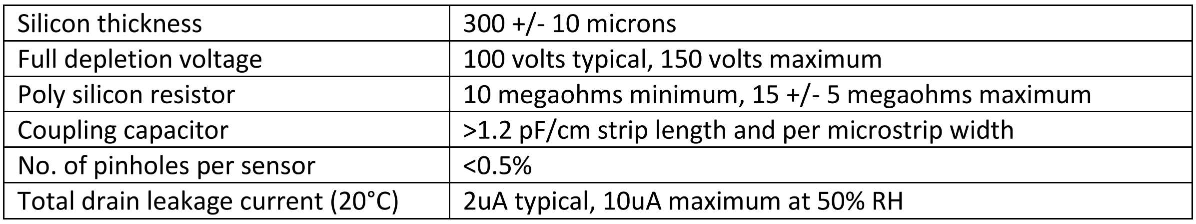

Silicon thickness	300 +/- 10 microns
Full depletion voltage	100 volts typical, 150 volts maximum
Poly silicon resistor	10 megaohms minimum, 15 +/- 5 megaohms maximum
Coupling capacitor	>1.2 pF/cm strip length and per microstrip width
No. of pinholes per sensor	<0.5%
Total drain leakage current (20°C)	2uA typical, 10uA maximum at 50% RH

Figure 5.10.: Specifications arranged between HEPHY and Micron.

6. Measurement results and statistical analysis

The Belle II Micron sensors were measured electrically in the QTC (described in the previous section) to determine their quality. Both electrical as well as mechanical and optical measurements methods were used.

To obtain significant results, different statistical methods were used to analyze the measurement results. The goals were on the one hand to determine the quality of the trapezoidal Micron sensors measured in Vienna and Trieste and on the other hand to compare the HEPHY measurement results to those obtained at INFN in Trieste. Moreover systematical deviations were sought for to gain information about differences in the measurements in Vienna and Trieste.

6.1. IV curves

6.1.1. Vienna

Figure 6.1 shows the IV curves of the sensors measured in Vienna. As explained in the former chapter while measuring the IV curve the bias voltage was ramped up in steps of 5 V to 200 V. It can be seen that the sensor 3084-10 reaches the compliance very fast. Our explanation is that there is possibly a crack in the sensor that leads to the very early breakthrough at 25 volts. It had been measured before with a good IV curve, but the last results show this very early breakthrough. The sensor 3048-1 has a very high leakage current reaching the compliance already at approximately 120 V. The sensor 3067-25 shows almost linear behavior and therefore also reaches the compliance before the 200 V. The almost linear behavior can be explained by strips that broke through, so only the linear characteristic line of the poly resistance can be seen. Since the operating voltage of the SVD is at 100 V this is not a problem and the sensor was nevertheless accepted. The curve of the sensor 3067-4 has a very flat incline, this means that the sensor has a high poly resistance. The declines of the curves of the sensors 3067-16 and 3077-10 at high voltage must be due to an error during the measurement, it can not be explained physically.

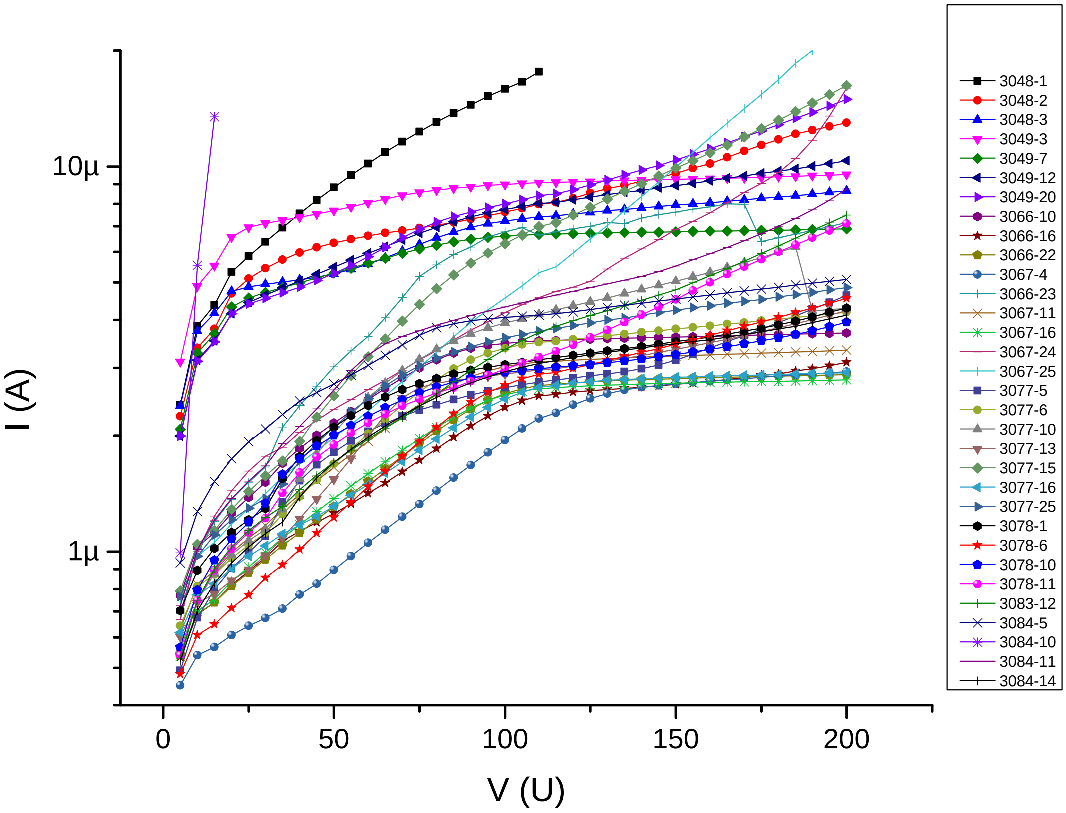

Figure 6.1.: IV curve measured of the Viennese sensors.

6.1.2. Trieste

Figure 6.2 shows the IV curve of the sensors tested in Trieste. The IV curves were measured in Trieste, therefore the bias voltage was this time ramped up in steps of 1 V to a maximum voltage of only 100 V. It can be seen that all three sensors of batch 3048 have a curve on a pretty high level. There is no breakthrough, but the values for the dark current are close to the specified limit. The three sensors were accepted, but nevertheless only rated with the mark B because of their high dark current. All of the other sensors show a very uniform behavior with dark currents at 100 V of around 2 to 3 μA. There was obviously an error in the measurement of the first points of the sensor 3084-8.

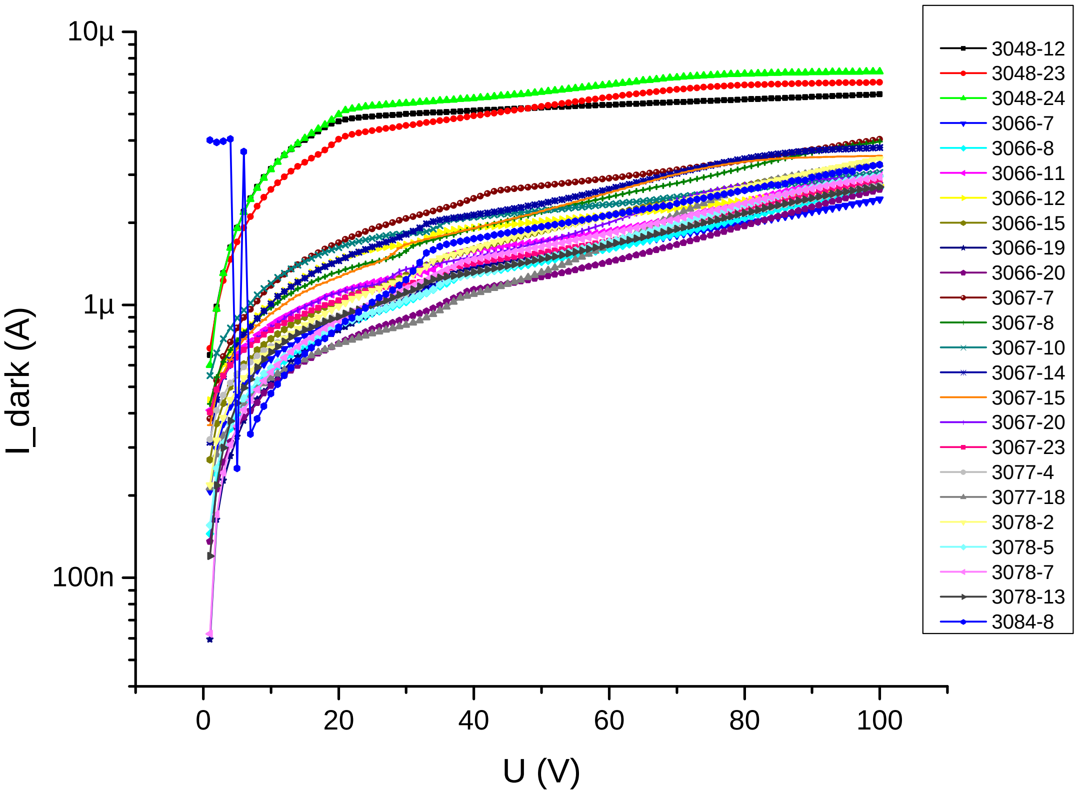

Figure 6.2.: IV curves measured in Trieste.

6.2. CV curves

6.2.1. Vienna

Figure 6.3 shows the CV curve of the sensors measured in Vienna. For that curve the bias voltage was ramped up in steps of 5 V up to 150 V. It can be seen that the depletion voltage (the voltage where the bulk material is fully depleted and the capacitance reaches its minimum) ranges between 20 and 40 V.

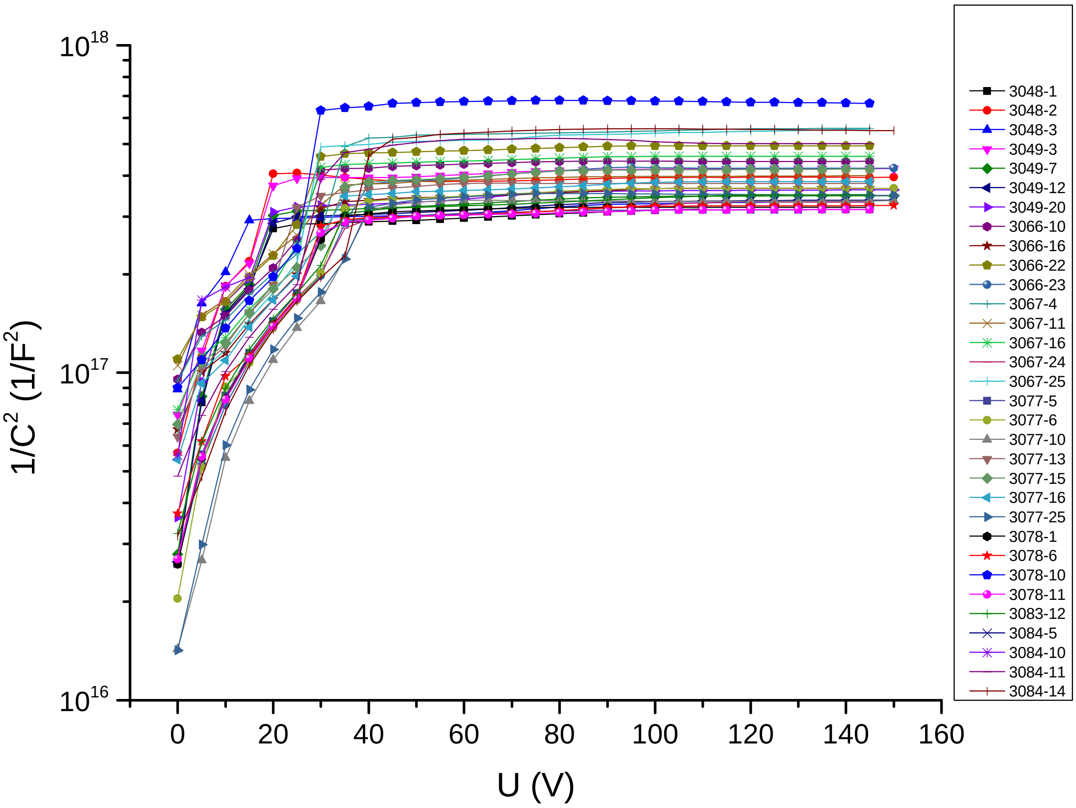

Figure 6.3.: CV curves measured in Vienna.

6.2.2. Trieste

The scan to obtain the CV curve was not done in Trieste. Nevertheless the values of the full depletion voltage were determined. A graphical display as histograms can be seen on in chapter 6.8.

6.3. Single strip current I_{strip}

An important tool for analysis was the histogram plot of all strip scan values. For every measured parameter (e.g. I_{strip}) all of the strips (for the n-side 512 × 54 = 27648, for the p-side 768 × 54 = 41472) were plotted in the histogram and then analyzed. The batches have been produced by Micron one after the other, 3048 being the first batch and 3084 the last one. The number after the batch (e.g. 3048-**1**) indicates at which time the sensor was produced in one certain batch. To gain information about how the sensor parameters differ over the different batches, sensors of the same batches are dyed in the same color.

The first tested parameter was the single strip leakage current. All in all, the results were satisfying, since all strips had currents of < 20 nA per strip, which were the specifications with Micron. Nevertheless the distributions were not very homogeneous for some of the sensors. Only the single strip scan results of the n-side could be fitted reasonably with a Gaussian curve.

6.3.1. n-side

Figure 6.4 shows the measurement results for I_{strip} of the sensors measured in Vienna. A clear peak can be seen between 2 and 3 nA and the distribution looks like an oblique Gaussian curve. On figure 6.5 (a) it can be seen that mostly the sensors from the very first batches 3048 and 3049 have high single strip currents. Nevertheless the values are inside the specifications (smaller than 20nA). Figure 6.5 (b) shows that the function can be reasonably well approximated by a Gaussian curve with a mean value of approximately 2.98 nA and a standard deviation (σ) of 1.07 nA. The adjusted R-square is called coefficient of determination and is a value for how good the fit is. The closer the fit is to the data points the closer the adjusted R-square will be to the value of one. It is at maximum 1 and for the given fit it is satisfactory with a value of 0.91.

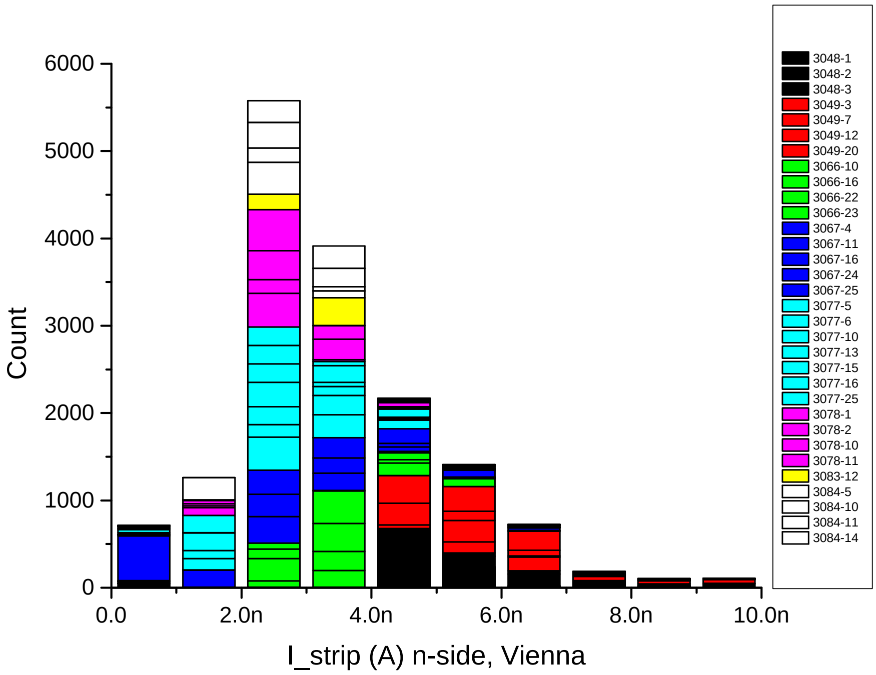

Figure 6.4.: Histogram I_{strip} n-side Vienna.

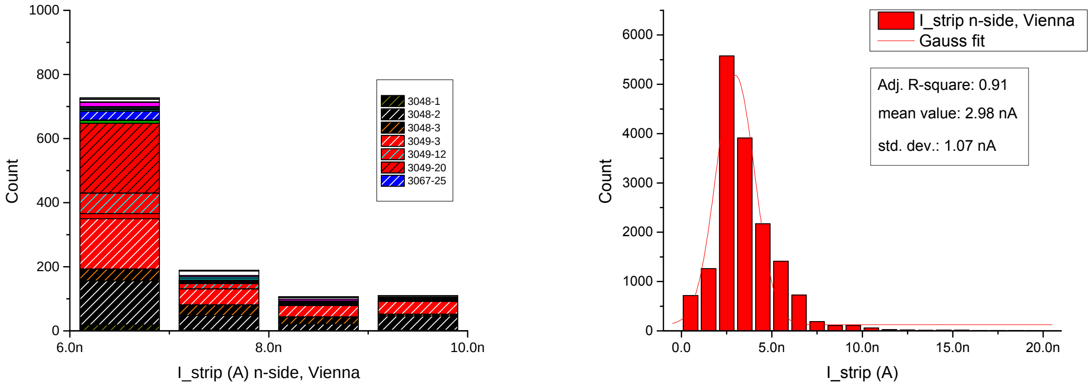

(a) Zoom in the higher single strip currents.

(b) Single strip current distribution fitted by a Gaussian curve.

Figure 6.5.: Single strip currents of n-side, tested in Vienna.

An introduction how to read the box plot can be found in section 4.5. On figure 6.6 it can be seen that the mean and the median of all of the single strip currents measured in Vienna is lower than 10 nA. Since the upper limit for the single strip current is at 20 nA, this is a good result. Also most of the boxes are rather small with a maximum width of 3 nA, this is also a quality feature of the Micron sensors. Only two sensors have a quite broad box, namely the sensor 3048-2 and the sensor 3049-3. Some of the maximum values are close to 20 nA but the maximum of the whiskers is only around 7 nA (except for the two mentioned sensors), so only some rare individual strips have a single strip current higher than 10 nA. Really good is the sensor 3078-11, having a very tight box and a very low maximum (thus no noisy strip at all). The sensors 3066-23 and 3077-10 have a significantly higher mean that median value which indicates that there are some outliers with higher current.

The histogram of the single strip measurements for the Trieste sensors (see figure 6.7) has also a peak at around 3 nA. Some of the sensors have higher single strip currents, first of all the sensor 3067-8. We assume that there must have been some systematical error in the measurements in Trieste, since the given sensor has a pretty low leakage current. And the sum of the single strip current must normally be a lower limit for the full sensor leakage current. Again the sensors of the very first batch 3048 have very high single strip currents. And finally the sensor 3078-13 has a I_{strip} slightly below 10 nA. There was no sense in doing a Gaussian fit since the distribution didn't look Gaussian at all.

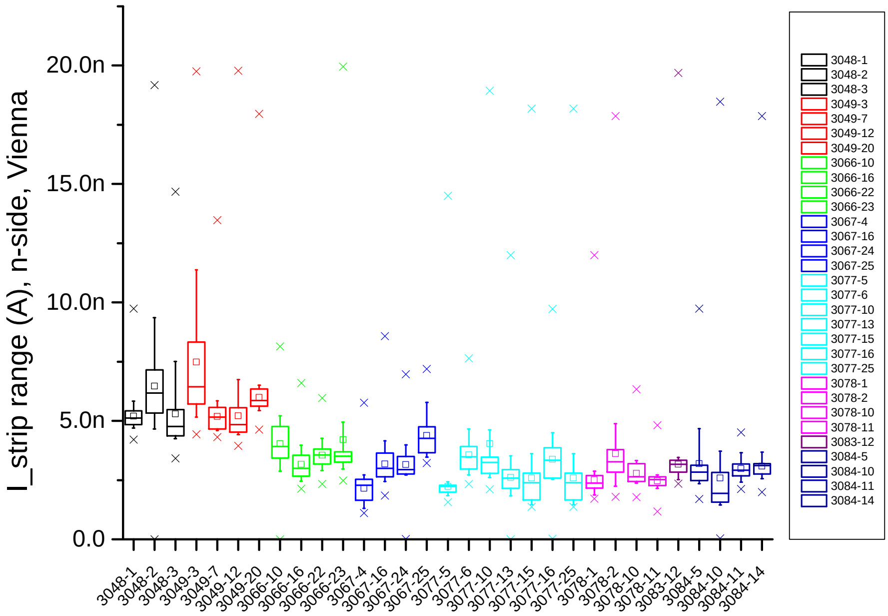

Figure 6.6.: Box plot I_{strip} n-side Vienna.

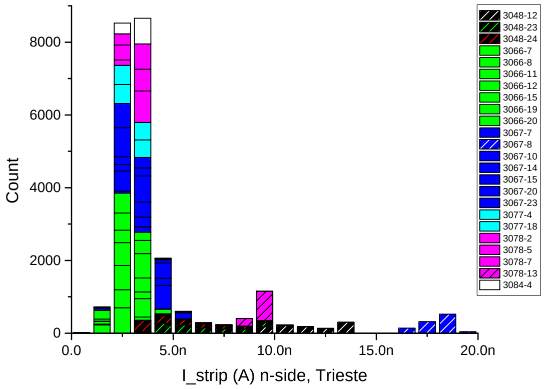

Figure 6.7.: Histogram I_{strip} n-side Trieste.

Figure 6.8 shows the box plot for I_{strip} and the sensors measured in Trieste. It shows again that the sensor 3067-8 has very high single strip currents with almost 20 nA. For this sensor the whole range, minimum to maximum lies between 15 and 20 nA. As already mentioned there was most likely a mistake in the measurements in Trieste because the IV curve (see figure 6.2) shows a rather low dark current. A lower limit for the dark current of a sensor is the sum of the single strip currents. If the sensor 3067-8 really has single strip currents of about 15 nA, then the whole sensor would have a leakage current of at least 15 nA × 512 ∼ 8 μA. Since it only has a dark current of 4 μA (see figure 6.35 , there must have been a mistake in the I_{strip} measurements. There is one other sensor with a high single strip current, the sensor 3048-12. It has also a high dark current and was therefore B graded. It can be seen that the whole 3048 batch has rather high single strip currents. They also have rather high dark currents and were therefore all graded B or even rejected. The sensors of the batch 3048 also have very large boxes, which indicates a lower quality, since homogeneous single strip currents are a quality feature of a sensor. The sensor 3078-13 has also significantly higher strip currents than the rest of the same batch- this is not big a problem since its dark current is only 3 μA.

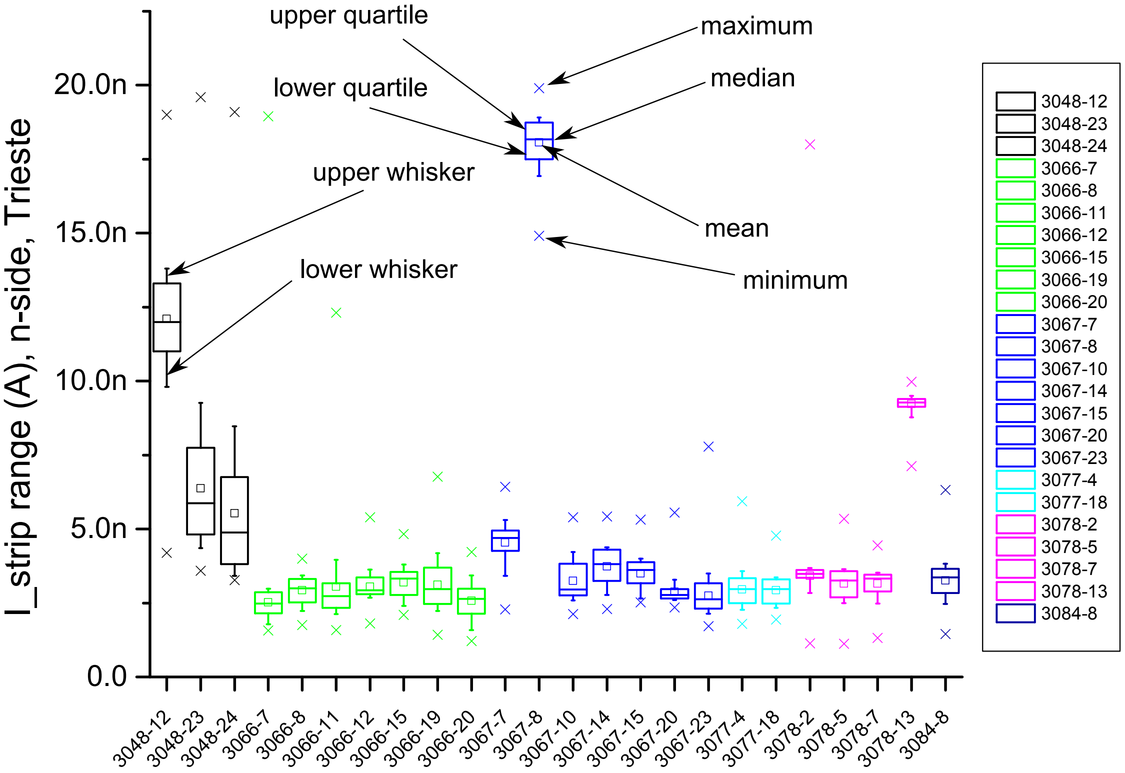

Figure 6.8.: Box plot I_{strip} n-side Trieste.

Figure 6.9 shows all sensors (Viennese and Trieste measurements in one graph). Concerning the single strip current on the n-side the batches with the best quality were the batches 3066, 3077, 3083 and 3084. The histogram was fitted by a Gaussian curve, the average value respectively the center of the Gaussian curve is 3.00 nA and the standard

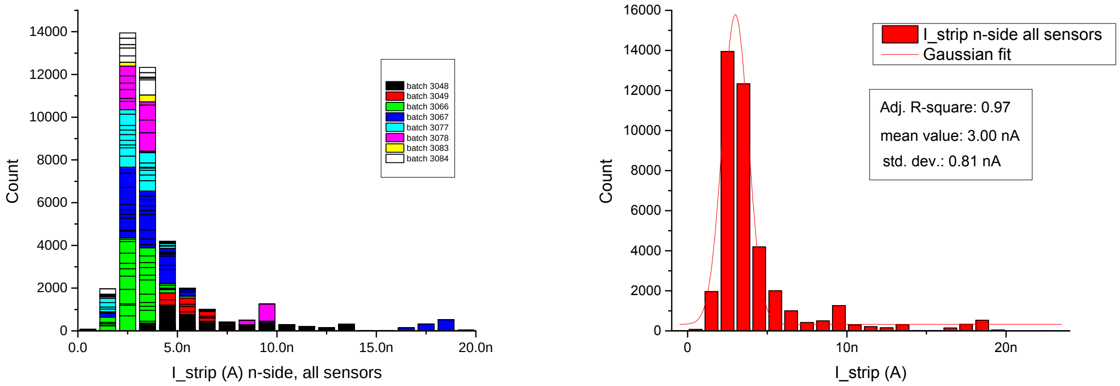

(a) Histogram I$_{strip}$ n-side all sensors.

(b) Single strip current distribution of all sensors fitted by a Gaussian curve.

Figure 6.9.: Single strip currents of all sensors, n-side.

deviation σ is 0.81 nA. The fit is pretty good, since the adjusted R-square is almost 1 (0.97). The skewness of the given curve is 2.9, which indicates that the right tail is longer. The kurtosis is pretty high with 9.2, so the graph is leptokurtic and the distribution is pointier than the standard Gauss distribution. This indicates, as expected that the single strip currents are randomly distributed variables.

6.3.2. p-side

The next measured parameter is the single strip current for the p-side. Figure 6.10 shows a comparison of the results in Trieste and in Vienna. It can be seen at the first glance that the distribution of the Viennese measurements is much broader than the one of the tests in Trieste. While the sensors measured in Trieste didn't have high single strip currents (the maximum is 6 nA), the sensors tested in Vienna have maximum values of 14 nA. Figure 6.11 shows that especially the sensors produced during the first batches (3048 and 3049) have very high strip currents. It is interesting that the sensors of batch 3048 that were tested in Trieste don't show the high strip currents that the sensors of batch 3048 tested in Vienna have. This can probably be explained by the fact that the Viennese sensors have very low numbers in the batch (3048-1 until 3048-3) in comparison to the high numbers of the sensors measured in Trieste (3048-12, 3048-23, 3048-24). But it is also interesting that the next sensors produced after that (batch 3049) have high single strip currents again. All measured sensors in one graph can be seen on 6.11 (b). There was a (pretty good) Gauss fit performed with a mean value of 1.62 nA and a standard deviation of 0.51 nA.

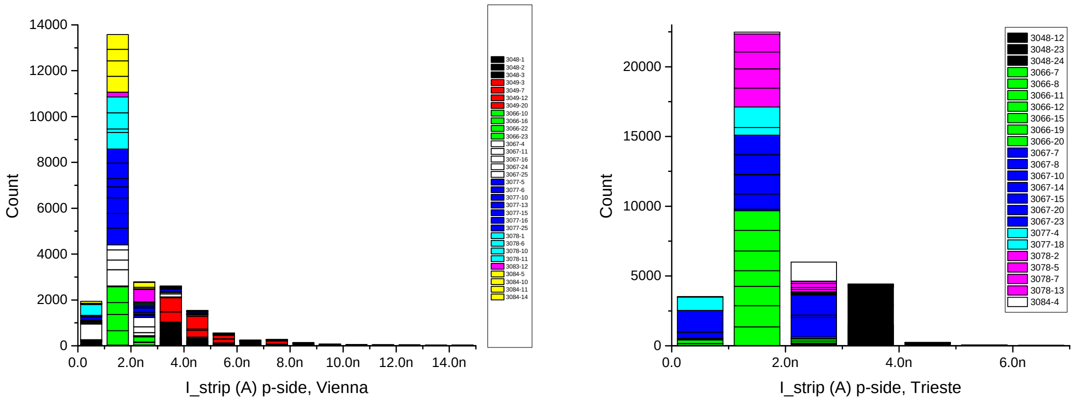

(a) Single strip current p-side, Vienna.

(b) Single strip current p-side, Trieste

Figure 6.10.: Single strip currents of p-side, Vienna and Trieste.

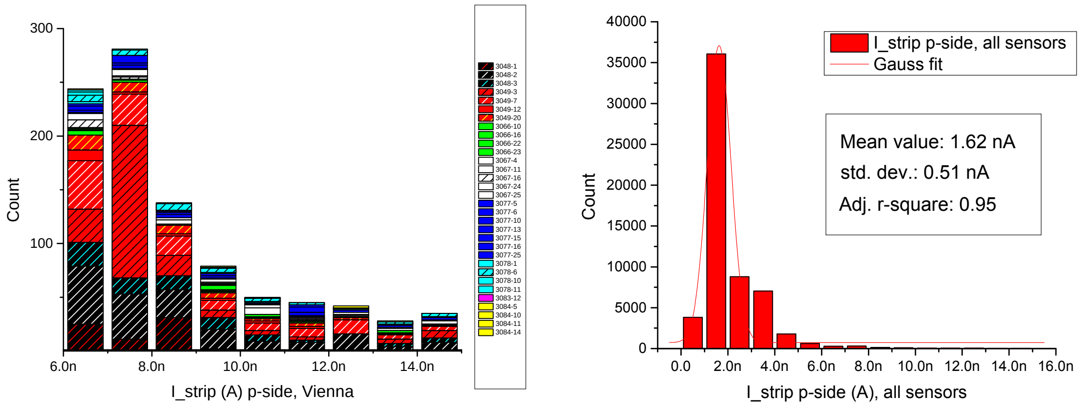

(a) Zoom in the single strip currents higher than 6 nA, p-side, Vienna.

(b) Single strip current of all tested sensors fitted by a Gauss curve, p-side.

Figure 6.11.: Single strip currents of p-side, Vienna and all sensors.

Figure 6.12 shows a box plot of the single strip currents of the p-side in Vienna. It can be seen that the boxes of the first batches are again generally broader than those of the later ones. Also some sensors perform very well again, like the sensor 3077-5 and the sensor 3084-10, with very slim boxes and few outliers. Nevertheless most of the maxima are above 10 nA, that indicates that almost every sensor had noisy strips. Looking at the box plot, the best performing batches for the single strip current on the p-side are batches 3066, 3078, 3083 and 3084.

Figure 6.13 (see page 57) is the box plot for the Trieste measurements. It can be seen that the boxes are much tighter than that of the Viennese tests. There is only one

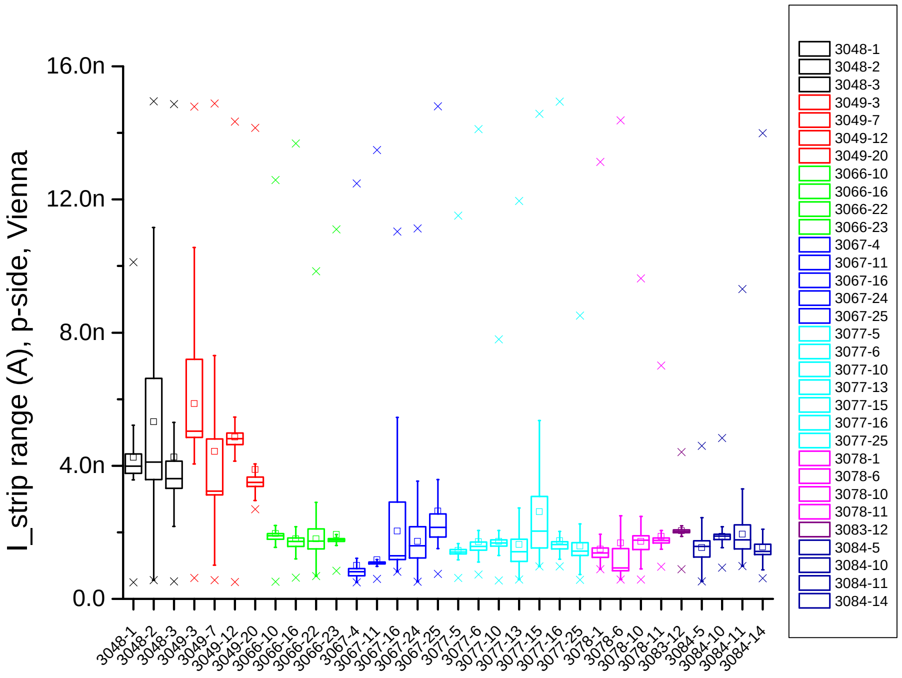

Figure 6.12.: Box plot I_{strip} p-side Vienna.

sensor with a slightly broader box, that is the sensor 3066-12. Some of the sensors have a minimum value of 0 nA, this indicates that there might have been contact problems during the measurements in Trieste. In general also the mean and the median values are much lower than that of the Viennese sensors. It can be nevertheless seen that also for the Trieste sensors the single strip currents of the batch 3048 were higher than the rest of the currents.

6.4. Poly silicon resistance R_{poly}

The next measured parameter was the poly resistance (the poly crystalline silicon bias resistors). The measured values reached from 5 MΩ to 50 MΩ. The big differences in the poly resistances can be most probably explained by the production process of the silicon resistances.

6.4.1. n-side

Figure 6.14 show the curves of the poly resistance for the sensors measured in Vienna and Trieste. The distribution of the sensors tested in Vienna looks similar to a Gaussian curve, the histogram of the sensors measured in Trieste doesn't. It is interesting

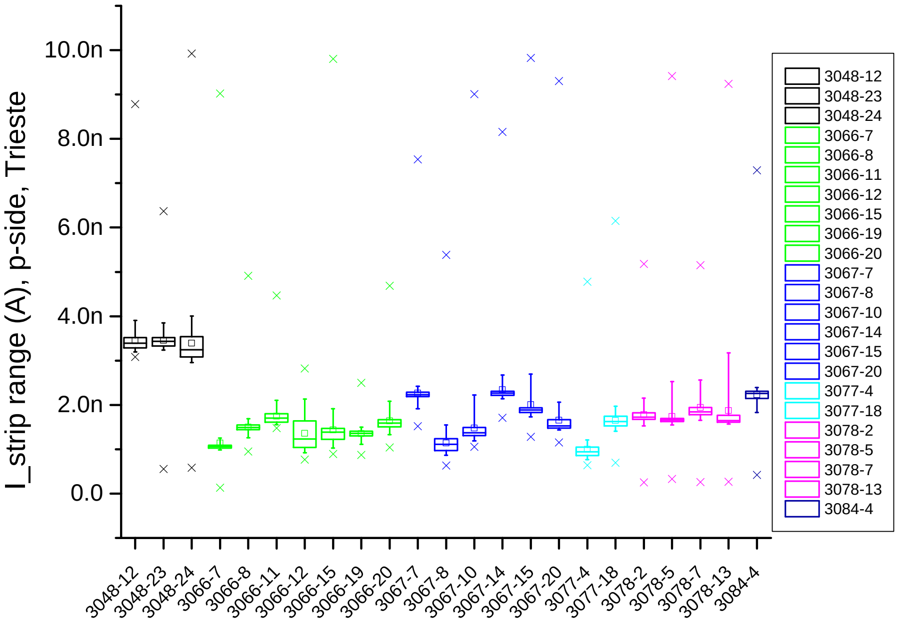

Figure 6.13.: Box plot I$_{strip}$ p-side Trieste.

that the measured poly resistances reach 50 MΩ for the measurements in Vienna and that the maximum is only around 30 MΩ for the Trieste sensors. While the Trieste measurements peak between 10 and 12 MΩ, the Viennese measurements peak between 16 and 18 MΩ. Figure 6.15 (a) shows the results for all measured sensors together in one histogram. Again, the distribution is not at all Gaussian, so there is no gain by fitting it with a Gaussian curve. Figure 6.15 (b) shows a zoom in the resistances higher than 30 MΩ that were measured. It can be seen that the last produced batch 3084 has three sensors with high poly resistances. Also the batch 3067 has two sensors with high R$_{poly}$ and finally the sensor 3078-10. All of those sensors were accepted nevertheless.

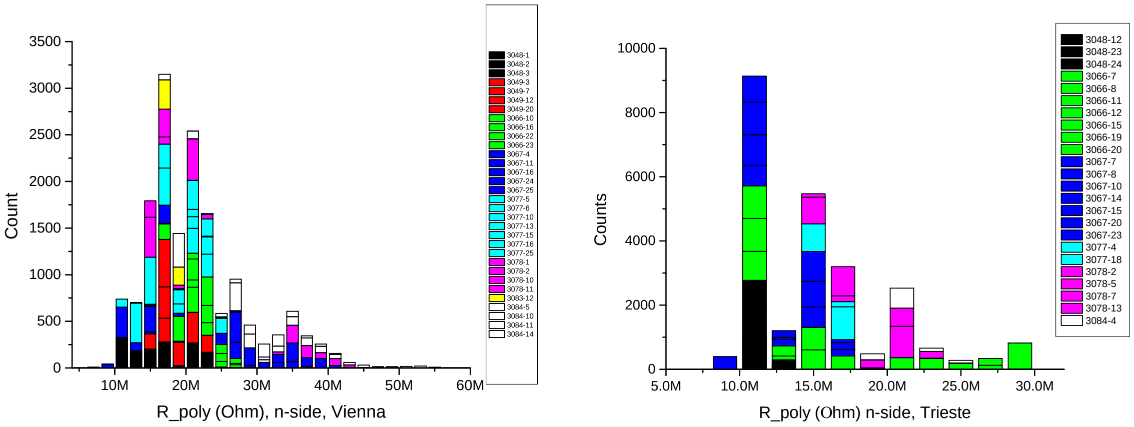

(a) Histogram R_{poly} n-side, Vienna.

(b) Histogram R_{poly} n-side, Trieste.

Figure 6.14.: Poly resistors of the sensors in Vienna and Trieste.

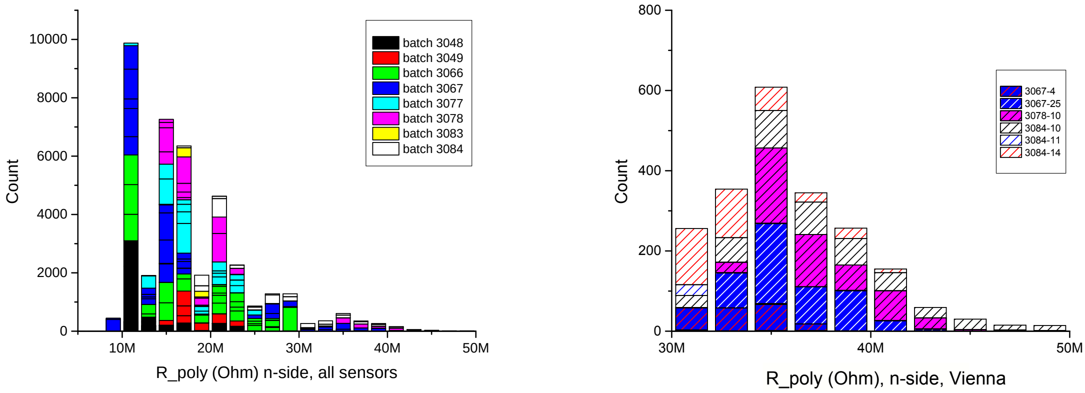

(a) Histogram R_{poly} n-side, all sensors.

(b) Histogram R_{poly} n-side, Vienna.

Figure 6.15.: Poly resistors of the sensors in Trieste and of all sensors, n-side.

Figure 6.16 shows the box plot for the poly resistances on the n-side measured in Vienna. It can be seen that they vary between 5 and almost 60 MΩ. Most of the sensors have rather narrow boxes, only the sensors 3084-10, 3067-4, 3067-25 and 3078-10 and 3084-14 have broader boxes. It can be seen that the value of the poly resistance depends on the batch number, for example batch 3067, batch 3078 and batch 3084 tend to have higher poly resistances. Nevertheless in batch 3067 there is also the lowest box of all Viennese measurements, with a mean and a median of approximately 10 MΩ. It can be seen although that some batches have more homogeneous values than others. For example the batches 3048, 3049, 3078 and 3083 do not vary as much as the other batches, which is a quality feature.

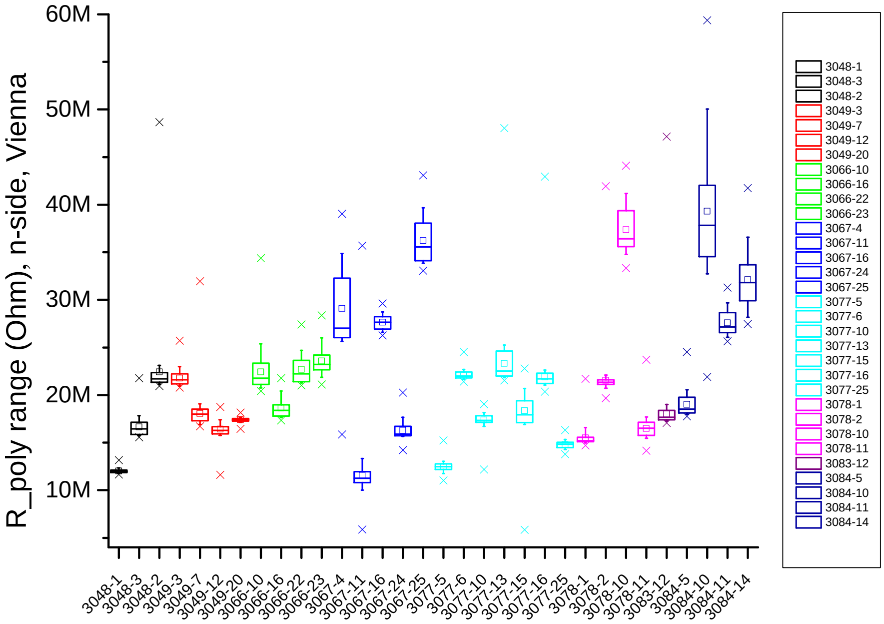

Figure 6.16.: Box plot R_{poly} n-side Vienna.

Let's take a look at the box plot of R_{poly} of Trieste (see figure 6.17). It can be seen that the later batches 3078 and 3084 have significantly higher means and medians than the rest of the batches. Also there are two sensors of batch 3066 (3066-8 and 3066-20) that have much higher poly resistances than the rest of the batch. It is interesting that the sensors of batch 3048 that didn't perform well for the single strip currents have very narrow boxes and very homogeneous values of 10 to 12 MΩ, which is a quality feature.

6.4.2. p-side

Figure 6.18 shows the measurement results for the poly resistance of the tests in Vienna and Trieste. The Viennese values are between 5 and 40 MΩ, whereas the Trieste results reach from 10 to 45 MΩ. The Viennese results aren't homogeneous at all, there are in total four big peaks, between 10 and 12, between 12 and 14, between 16 and 18 and between 20 and 22 MΩ. There is also a little peak between 32 and 34 MΩ. So it doesn't remind of a Gaussian curve at all. For the tests made in Trieste there are also three peaks, between 14 and 16 MΩ, between 18 and 20 MΩ and between 28 and 30 MΩ. High resistances (over 30 MΩ) were found on the sensors 3067-4, 3066-22, 3078-10 and 3084-10 (Vienna) and for the sensors 3048-23, 3066-7, 3066-12, 3066-19, 3066-20, 3067-8 and 3067-10 (Trieste). In the Trieste results there were no sensors with high values in the latest batches 3077 till 3084.

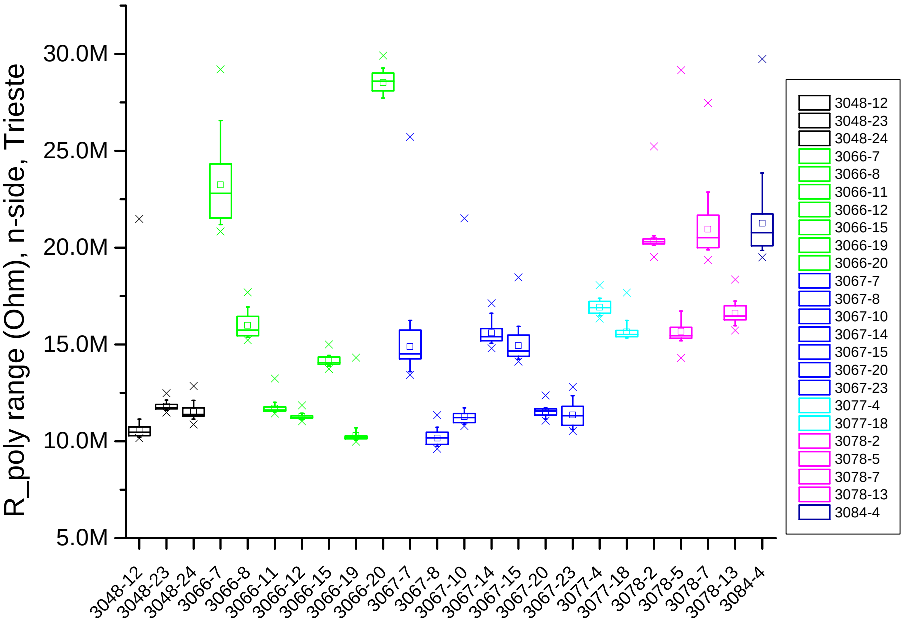

Figure 6.17.: Box plot R$_{poly}$ n-side Trieste.

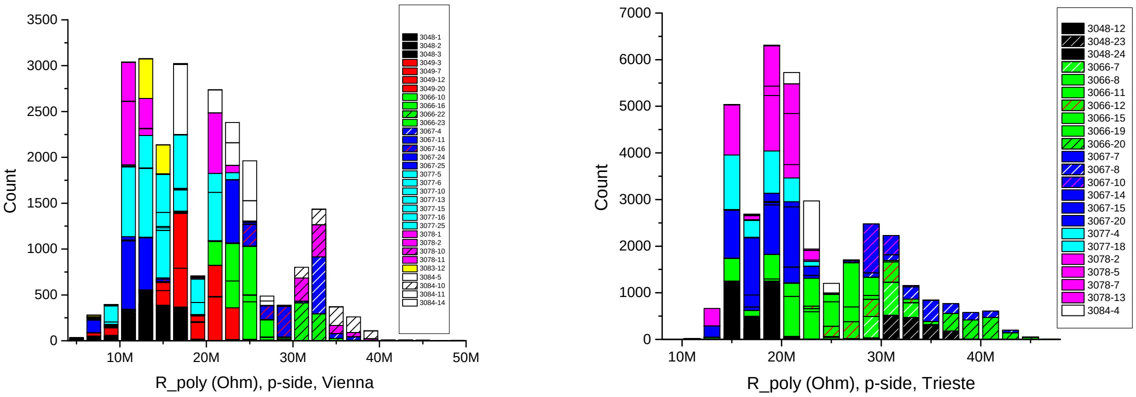

(a) Histogram R$_{poly}$ p-side, Vienna.

(b) Histogram R$_{poly}$ p-side, Trieste.

Figure 6.18.: Poly resistors of the sensors in Vienna and Trieste, p-side.

Figure 6.19 shows the histogram of R$_{poly}$ for all strips of all measured sensors. It can be fitted by a Gaussian curve see (b), even though the fit is not very good. The value adjusted R-square is at 0.79 for the given fit. The average value of the Gaussian is

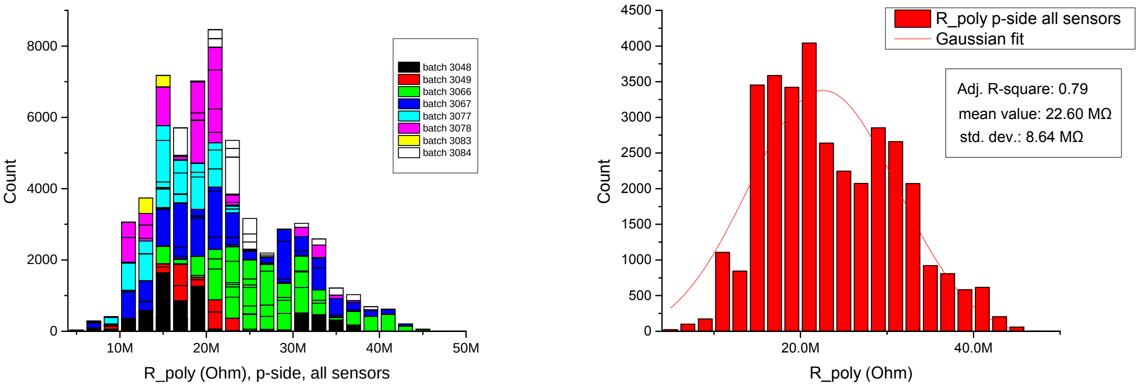

(a) Histogram R$_{poly}$ p-side, all sensors.

(b) Histogram R$_{poly}$ p-side, all sensors, fitted by a Gaussian curve.

Figure 6.19.: Histogram poly resistance of all sensors, p-side.

22.60 MΩ and the standard deviation σ is pretty high with 8.64 MΩ. So only 68.27% of all the measured strips are in the range between 22.6 ±8.6 MΩ, so between 14 and 31.6 MΩ. The skewness is 0.36 for the given fit, so the distribution is almost symmetrical. The kurtosis is -0.53 and so smaller than the kurtosis of the Gauss function- therefore the curve is platokurtic and flatter than the standard Gauss curve. Comparing the fit with the Gaussian curve of the n-side (see figure 6.20), it can be seen that the poly resistance values behave even much less like a Gaussian curve for the n-side. The value adjusted R-square that is a value for how good a fit is, is 0.79 for the p-side and only 0.56 for the n-side. Only the standard deviation (with 4.8 MΩ) is smaller for the fit of the n-side, so the Gaussian curve for the p-side is broader. Nevertheless one can not really draw any conclusions out of this fact, since both fits are not very accurate.

Looking at figure 6.21, it shows the box plot of the poly resistance on the p-side of the sensors measured in Vienna. The sensor 3077-15 pops instantly into the eye, because it has a very large box, reaching over 10 MΩ. In general, the means of the sensors vary between 12MΩ (3048-1) and 35 MΩ. Again the last batch 3084 has rather high poly resistances. It is interesting that the sensor 3084-14 that has a very tight box has also outliers until almost 60 MΩ. In general it can be seen that the poly resistances vary a lot. This can be most probably explained by the following: The poly resistances are made of doped silicon that is meander-shaped. The silicon for the resistances is only slightly doped because it needs to have a very high resistances of about 10 MΩ. Since the resistance should still stay high (10 MΩ), the doping atoms should only be shot at the silicon for a very short time. Slight variations of the doping time might result in a high difference of the poly silicon resistance- that's how the inhomogeneous results for this parameter (that will be also seen for the Trieste measurements) might be explained.

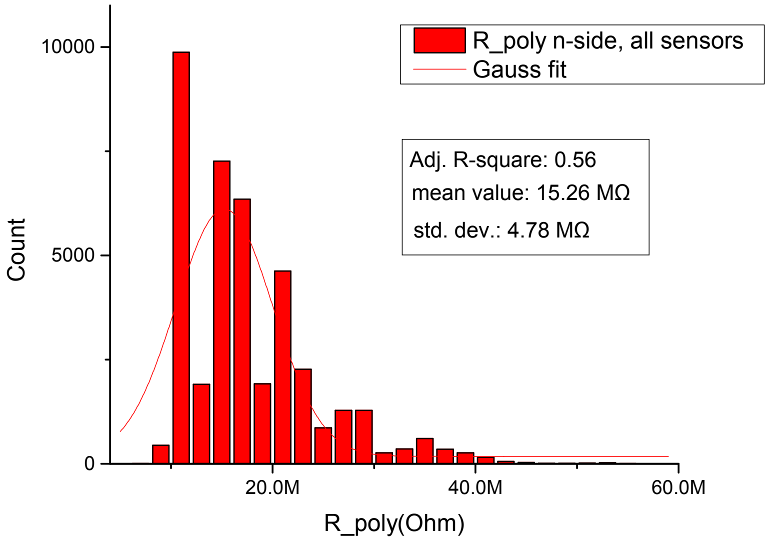

Figure 6.20.: Histogram of R_{poly} and all measured strips, fitted with a Gauss curve.

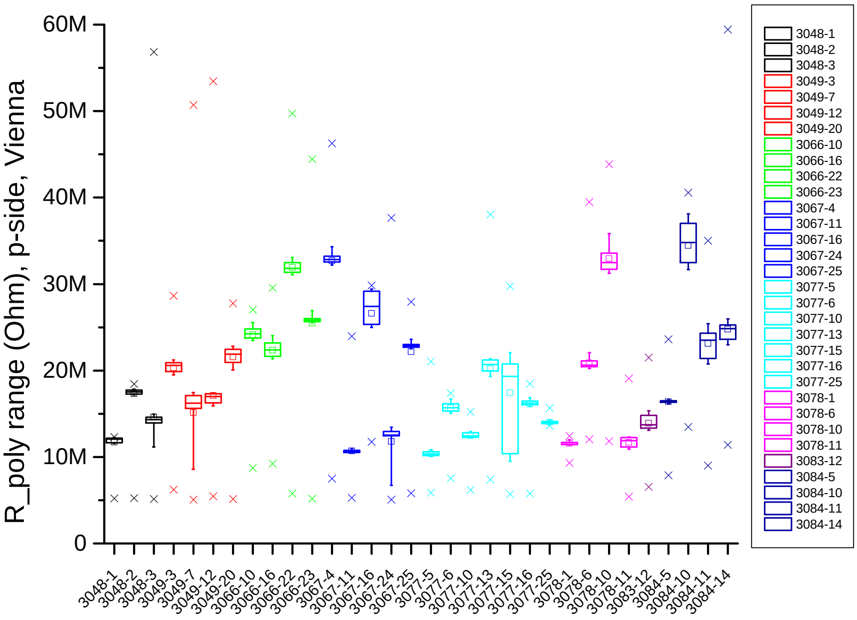

Figure 6.21.: Box plot R_{poly} p-side Vienna.

Figure 6.22 shows the box plot of the p-side of the sensors measured in Trieste. It can be seen that some of the sensors have pretty large boxes, mostly some of batch 3066, but also the sensor 3048-23 and the sensor 3067-8. There are some sensors with very high means and medians, again mostly of batch 3066, the sensor 3048-23 and the sensor 3067-8. The batches 3077, 3078 and 3084 show very homogeneous results, with means between 10 and 20 MΩ, which is a quality feature of those batches. In general the poly silicon resistance varies between 10 MΩ which is (as expected) about the same range of the measurements in Vienna.

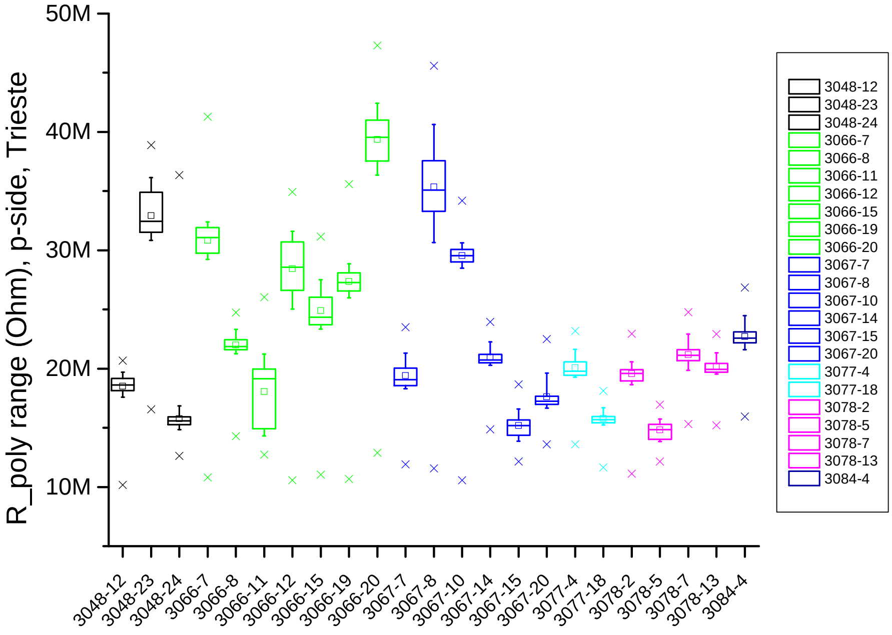

Figure 6.22.: Box plot R_{poly} p-side Trieste.

6.5. Coupling capacitance C_{ac}

The next determined parameter was the coupling capacitance. Its values should have been > 1.2 pF per cm strip length and per μm strip width. So the measured values were divided through the strip length and the strip width. This was done to be able to better compare the measured values to each other, since the strip length differs on both n and p-side and the strips on the p- and n-side have different strip widths. In a typical coupling capacitance measurement of the n-side the value of C_{ac} is monotonically increasing, as can be seen on figure 5.8 (c). By looking at the following histograms it can be seen that most of the sensors didn't fulfill those determined specifications.

6.5.1. n-side

For the coupling capacitance on the n-side both the measurements in Vienna and in Trieste could be very well approximated by a Gauss function. It can be seen on figures 6.23 (a) and (b). The adjusted R-square is 0.96 for the fit of the Trieste data and even 0.99 for the fit of the Viennese measurements. The mean value is close to the specifications with 1.18 μF/cm/μm for the Trieste sensors. For the Viennese measurements the mean value is only 0.98 μF/cm/μm. As can be seen on the very slim curve the standard deviation is very small for the Viennese measurements with only 25 nF/cm/μm. The Trieste tests have a standard deviation that is approximately 7 times higher with 0.18 μF/cm/μm. The fitted curve of the Viennese measurements has a negative skewness of -8.0 which means that the left tail is longer and a very high kurtosis (66.3) which means that the distribution is much pointier than the standard normal distribution. The Trieste curve has also a negative skewness of -0.9 (so slightly left-tailed) and a positive kurtosis bigger than 3 (4.0), so it is pointy.

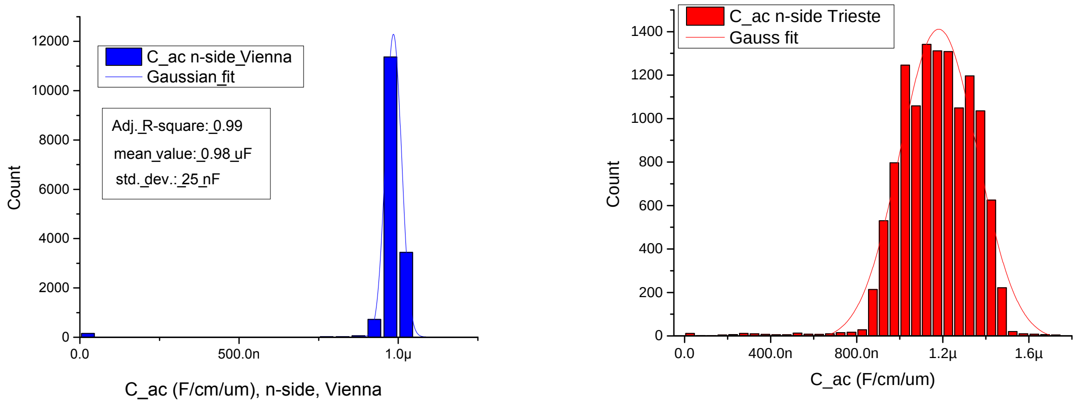

(a) Histogram C_{ac} n-side, Vienna with Gauss fit. (b) Histogram C_{ac} n-side, Trieste with Gauss fit.

Figure 6.23.: Coupling capacitance of the sensors in Vienna and Trieste, n-side, fitted by a Gaussian curve

The difference in the mean value and above all the standard deviation indicates systematical differences in the measurements in Vienna and Trieste, since it can be assumed that the sensors that were tested in Vienna and Trieste were randomly picked out. A method to test the systematical difference in the measurements is the independent two sample t-test (explanation see section 4.8). It can be used to determine if two sets of data are significantly different from each other or if the difference is only caused by a statistical fluke. A two-paired t-test was used, resulting in a t statistic of t=116 and a number of degrees of freedom of d.f.=19377 (equal variance not assumed, with Welch correction). In the 19377-dimensional two tailed t distribution the p-value is 0.00, which implies a very strong presumption against the null hypothesis that the two population means are equal. Since the sensors sent to Vienna and Trieste were picked out randomly, there has to be a significant difference in the measurement methods in Vienna and Trieste. It is assumed that the big difference in both the mean value and the standard deviation is due to the fact that the measurements in Trieste were carried out at both a different frequency and with a different amplitude. Whereas in Vienna the measurements were performed at a frequency of 100 Hz, in Trieste they were performed at 1 kHz. The amplitude used in Vienna was 250 mV and in Trieste they used an amplitude of 100 mV for the measurements. Another possibility is that the calibration of the LCR meter wasn't done properly before the measurements either in Vienna or Trieste. This would also be an explanation for the offset of 0.2 F/cm/μm.

Since there is such a big difference in the mean values, the graph of all measured sensors doesn't look Gauss-shaped. It can be seen on figure 6.24 (b). Figure 6.24 (a) shows the low capacitances (lower than 0.8 μF/cm/μm) of the Trieste measurements. It can be seen that except of the early batch 3048 all the batches are concerned. Nevertheless the highest column peaks at approximately 35 counts, so those outliers are very rare and thus not of significance.

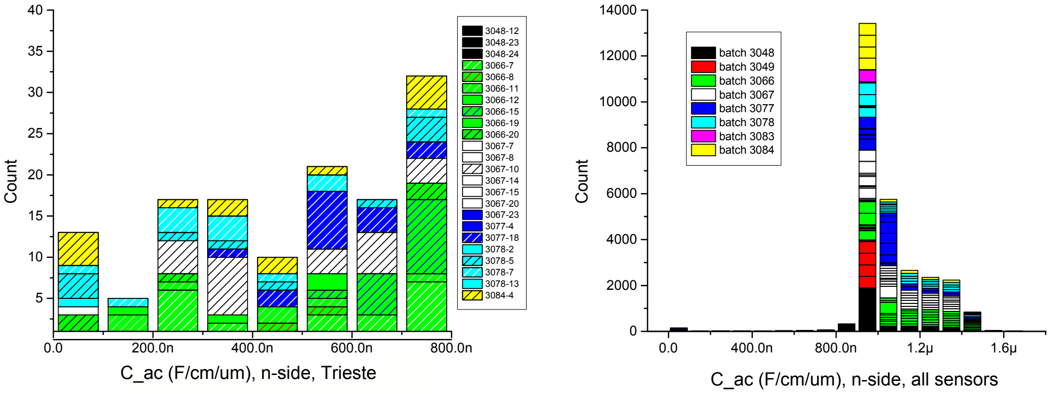

(a) Histogram C_{ac} n-side, Trieste, small capacitances.

(b) Histogram C_{ac} n-side, all sensors - not Gauss-shaped.

Figure 6.24.: Coupling capacitance of the measured sensors, n-side

The box plot of the n-side in Vienna 6.25 shows very tight boxes that have all a mean and median between 900 nF/cm/μm and 1.1 μF/cm/μm. So they are all lower than the value of 1.2 μF/cm/μm that has been arranged with Micron. The homogeneous distribution and the tight boxes are nevertheless quality features for the sensors.

Figure 6.26 is the box plot of the coupling capacitance of the n-side in Trieste. It can be seen that all of the sensors except the sensor 3048-12 are close to the specified values of 1.2 μF/cm/μm. Nevertheless that was specified as minimum value with Micron.

There is also a wider range between minimum and maximum for the Trieste results compared to the Viennese measurements. Anyway, the homogeneous distribution of both the Vienna and the Trieste plots are a quality feature of the sensors. It can be seen that the value of the coupling capacitance is distributed very homogeneously over the sensors.

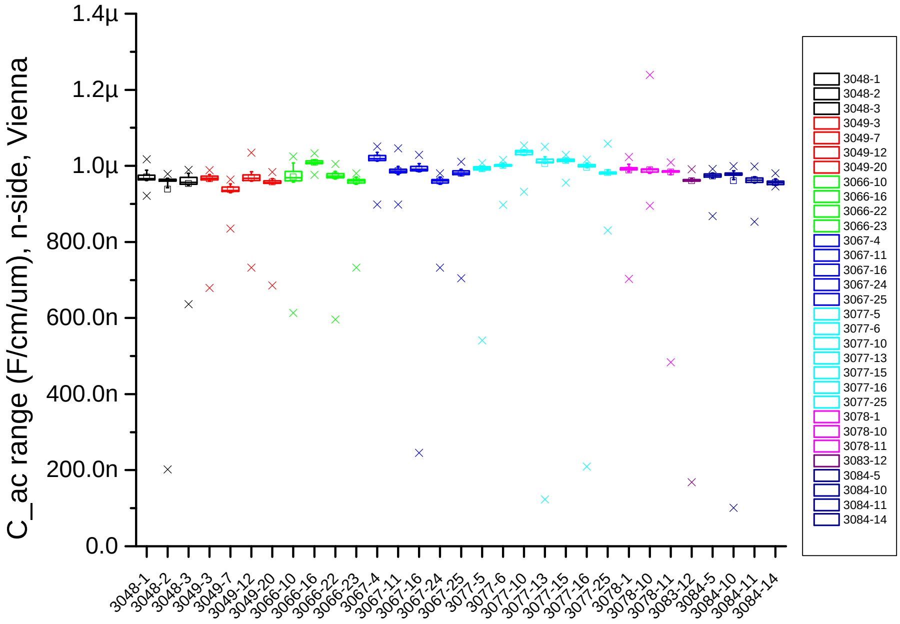

Figure 6.25.: Box plot C_{ac} n-side Vienna.

6.5.2. p-side

Coming to the p-side, the measurement results for the coupling capacitance of Trieste are very nicely Gauss shaped as can be seen on figure 6.27 (b). The adjusted R-square that is a value for the quality of a fit is 0.99 (the maximum is 1). The average value is 1.14 μF/cm/μm and the standard deviation very small with only 48 nF/cm/μm. The distribution of the coupling capacitance for the sensor strips measured in Vienna is much more inhomogeneous as can be seen on figure 6.27 (a) with a peak between 1.0 and 1.05 μF/cm/μm. The very low coupling capacitance values (0- 200 nF) can be most likely explained by a bad contact of the AC probe needle. The sensors with low C_{ac} values (between 200 and 800 nF) are of mostly of the very early batches 3048 and 3049 and also of the sensors 3066-10 and 3067-11. The sensor 3067-11 was rejected for its random C_{ac} values. Figure 6.28 shows the distribution for all the sensors tested, again it doesn't look very much like a Gaussian curve- nevertheless a Gauss fit was done. The mean value for the coupling capacitance for all sensors is 1.1 μF/cm/μm and the standard deviation σ

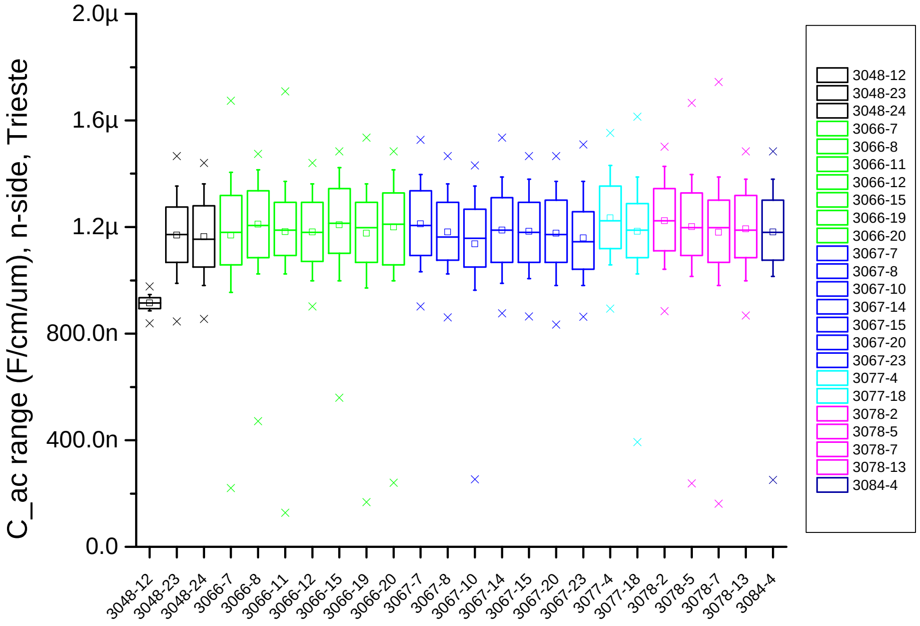

Figure 6.26.: Box plot C_{ac} n-side Trieste.

only 4.8 μF/cm/μm. The adjusted R-Square for this fit is 0.93, an indicator that the fit is pretty good. The skewness is 0.6, so the distribution is slightly right tailed and the skewness is 3.7 and so again pointier than the standard normal distribution.

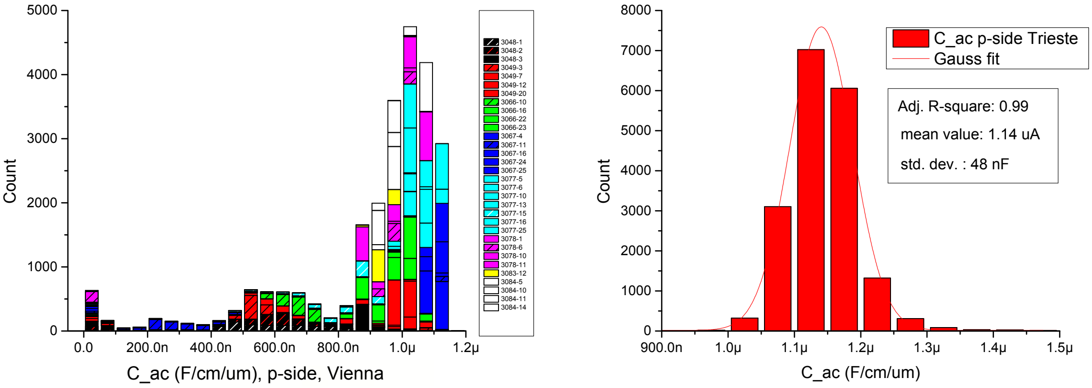

(a) Histogram C_{ac} p-side, Vienna.

(b) Histogram C_{ac} p-side, Trieste with Gauss fit.

Figure 6.27.: Coupling capacitance of the sensors in Vienna and Trieste, p-side.

Since there was such a (allegedly systematic) difference in the measurement results

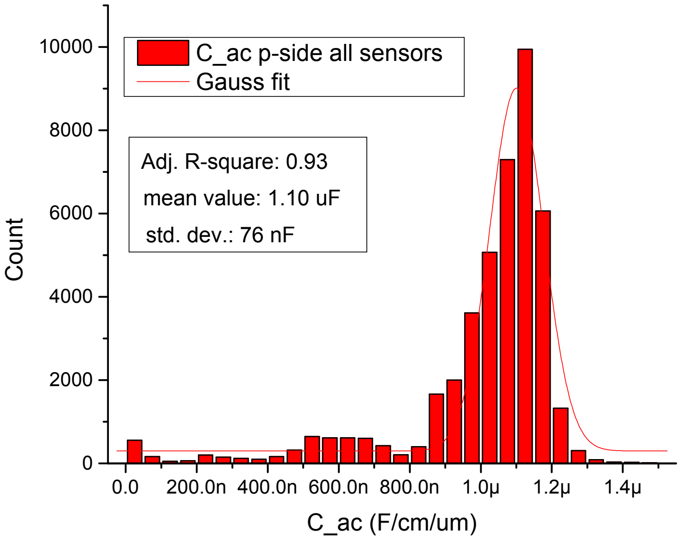

Figure 6.28.: Coupling capacitance p-side of all sensors, fitted by a Gauss curve.

the two paired t-test was performed again. As indicated in the former section this test determines if there is a systematical difference between two samples or if they could be part of the same probability distribution. This time again the probability for them to be in the same distribution was $p = 0.00$, which shows again that there are systematical differences in the measurement methods of Trieste and Vienna, at least as far as the determination of the coupling capacitance is concerned.

Figure 6.29 shows the box plot of the Viennese sensors. In general, the inhomogeneity that can be spotted at the first glance indicates a lower quality level for the coupling capacitance of the p-side. It can be seen that the sensor 3067-11 has very low values and was also therefore rejected. Also the sensors 3048-1, 3048-2 and 3049-3 have means and medians of lower than 600 nF/cm/μm, which is indeed a big difference to the specifications of >1.2 μF/cm/μm. Also large boxes have the sensors 3048-3, 3049-7 and 3077-15. The width of the boxes might be connected with problems during the measurements, but it has certainly also to do with the quality of the sensors, since the first two batches showed lower quality in almost all of the tests. Concerning this graph the batches coming off the best are the latest batches 3083 and 3084. In any case, the means and the medians of all sensors are here again significantly lower than the agreed specifications of larger than 1.2 μF/cm/μm.

The next box plot (see figure 6.30) shows the p-side results of Trieste. It can be seen that the distribution is much more homogeneous than the Viennese one. There is the sensor 3066-12 where the box is the largest, this is not a quality feature. In general, the results are very homogeneous again with means and medians between 1.1 and

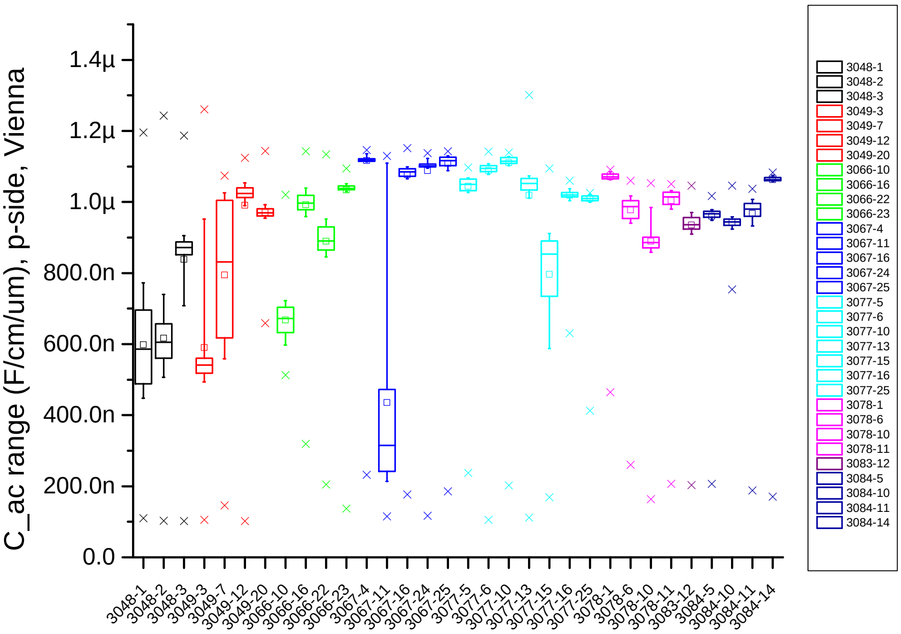

Figure 6.29.: Box plot C_{ac} p-side Vienna.

1.2 μF/cm/μm. It is interesting that in the Trieste measurements there were maximum values that were even higher than 1.4 μF/cm/μm.

In any case, also on the p-side there is a significant difference between the results of Vienna and Trieste. The Viennese results suggest that the quality of the coupling capacitance on the p-side is lower than on the n-side. The Trieste results are very similar for both n and p-side, so the inhomogeneity in the Viennese measurements might be also due to problems during the measurements. During the measurements of the p-sides there have been indeed problems with the contacting of the needle on the AC pad which made it necessary to perform a lot of remeasurements.

6.6. Number of pinholes/sensor

The next analyzed parameter was the number of pinhole per sensor. As mentioned in the former chapter, a pinhole is the worst defect a semiconductor sensor can have. At the strips with a pinhole the the charge can flow freely into the preamplifier, overloading the amplifiers of the main part of one whole chip. These strips must be identified and remain disconnected from the amplifier. A readout chip has 128 channels- if there are more than 5 pinholes in the 128 strips, the readout chip doesn't work at all. To be on the save side the specifications arranged with Micron were at maximum 0.5% pinholes.

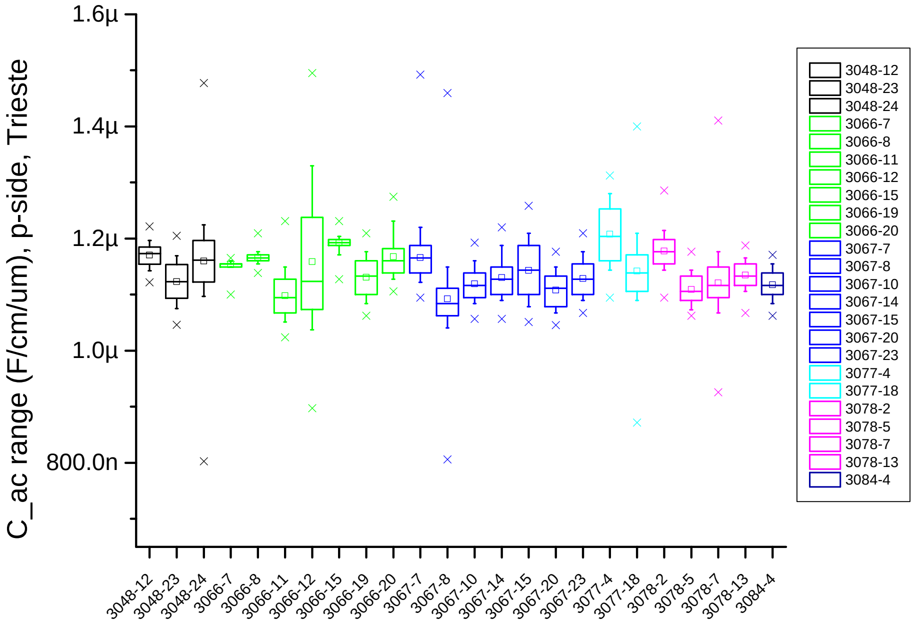

Figure 6.30.: Box plot C_{ac} p-side Trieste.

6.6.1. n-side

For the n-side, both the histogram of the pinholes of all sensors and the Trieste measurements show a maximum at 4 pinholes, for the Viennese tests the maximum is at 9 pinhole. Since there were many sensors with >0.5% pinholes the internal rejection limit was changed to <1% pinholes. In total, there is only one sensor exceeding the 1% limit, it is the sensor 3067-11 that was although already rejected because of random, much too low coupling capacitance values. Figure 6.31 (a) shows the plot for the n-side and for all 56 measured sensors. The separate results for the measurements in Vienna and in Trieste can be seen on figure 6.32.

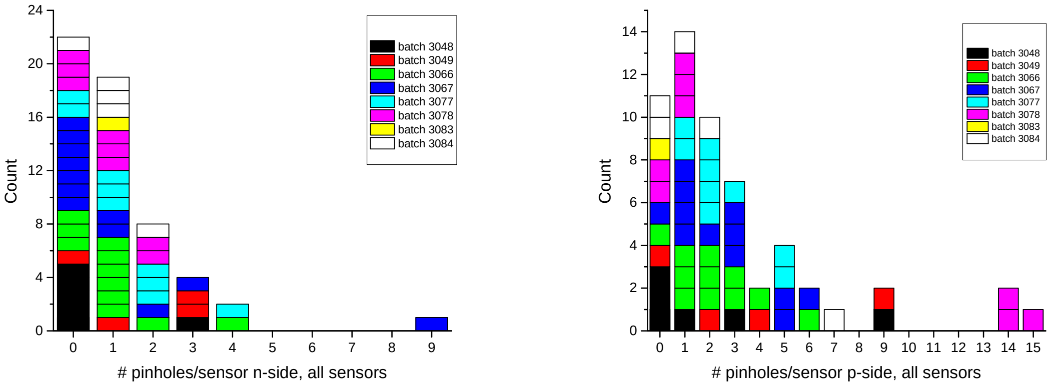

(a) Histogram of the number of pinholes per sensor, n-side, all sensors.

(b) Histogram of the number of pinholes per sensor, p-side, all sensors.

Figure 6.31.: Number of pinholes per sensor, n- and p-side.

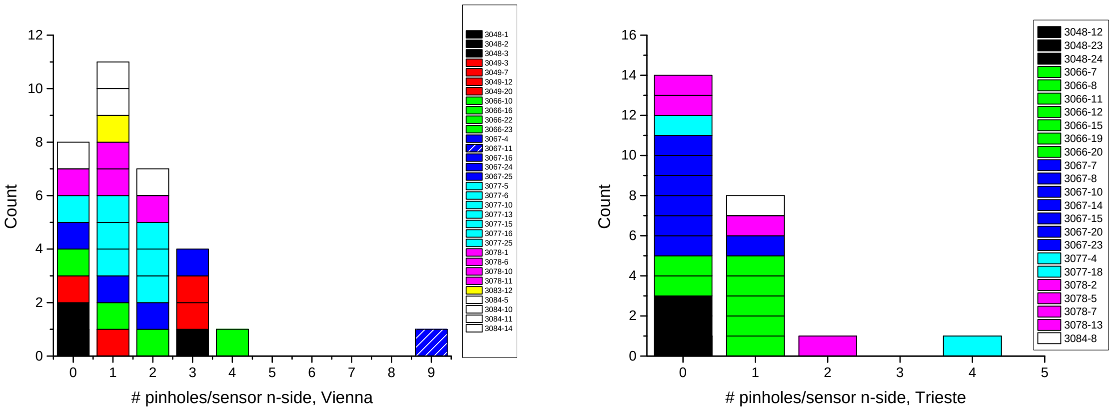

(a) Histogram of the number of pinholes per sensor, n-side, Vienna.

(b) Histogram of the number of pinholes per sensor, n-side, Trieste.

Figure 6.32.: Number of pinholes per sensor, n-side, Vienna and Trieste.

6.6.2. p-side

Figure 6.31 (b) shows the number of pinholes per sensor for the p-side and for all sensors. This time there are in total five sensors exceeding the percentage of 1% pinholes per sensor. As can be seen on figure 6.33 that shows the separate results for Vienna and Trieste it is the sensors 3078-1, 3078-2 and 3078-11, respectively 3048-3 and 3049-3. For the batch 3078 three out of 8 sensors have too many pinholes. The sensors 3066-23, 3067-8 and 3084-11 have 6 respectively 7 pinholes and are therefore only classified with the mark B.

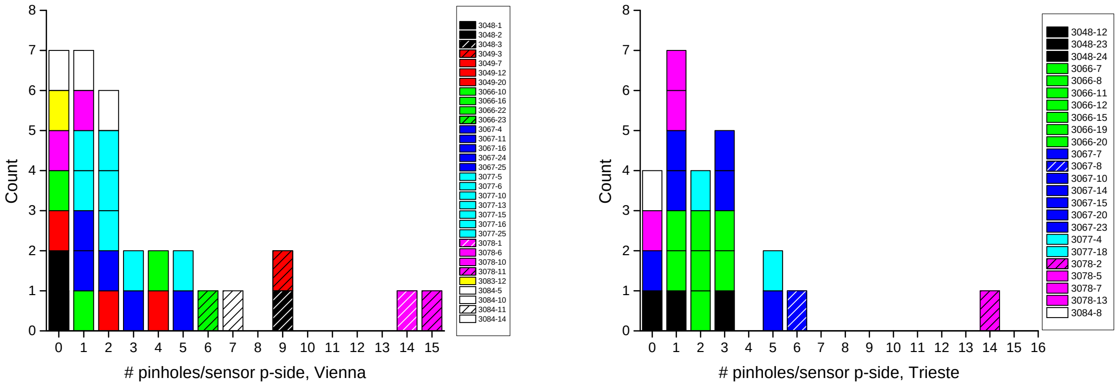

(a) Histogram of the number of pinholes per sensor, p-side, Vienna.

(b) Histogram of the number of pinholes per sensor, p-side, Trieste.

Figure 6.33.: Number of pinholes per sensor, p-side, Vienna and Trieste.

6.7. Total leakage current I_{dark}@100V

The dark currents of the sensors at 100 V were also measured and the results were plotted in histograms. As can be seen on figure 6.34 only one of the sensors exceeded the specification limit of 10 μA. It was the sensor 3048-1 that was therefore rejected for its too high dark current. All other sensors were inside the specifications. A clear peak can be seen between 2 and 3 μA and a much smaller peak between 6 and 8 μA. Figure 6.35 (a) shows the Trieste results- there are three sensors of the batch 3048 (with the number 12, 23 and 24) that are between 5 and 8 μA and so pretty close to the specification of 10 μA. Figure 6.34 (b) shows a Gauss fit of all sensors. The mean value is 2.9 μA with the standard deviation σ of 0.56 μA. The adjusted R-square is 0.91, so the fit is not that bad.

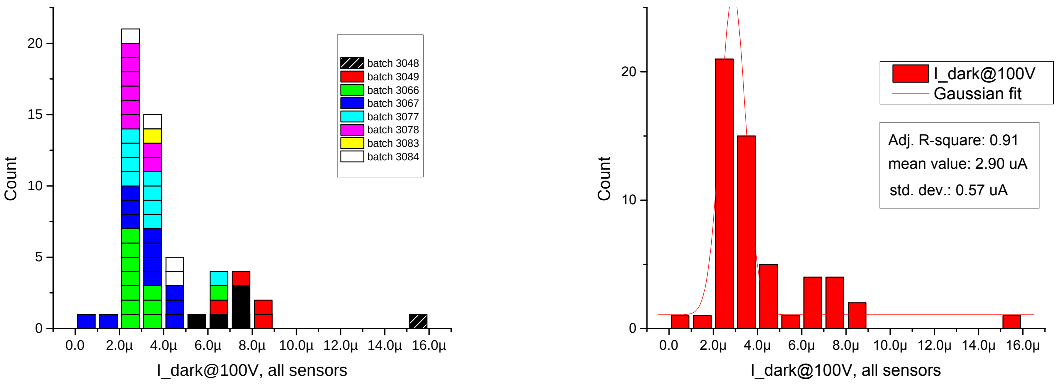

(a) Histogram of the dark current at 100 V, all sensors.

(b) Histogram of the dark current at V, all sensors with Gauss fit.

Figure 6.34.: Dark current of the sensors at 100 V.

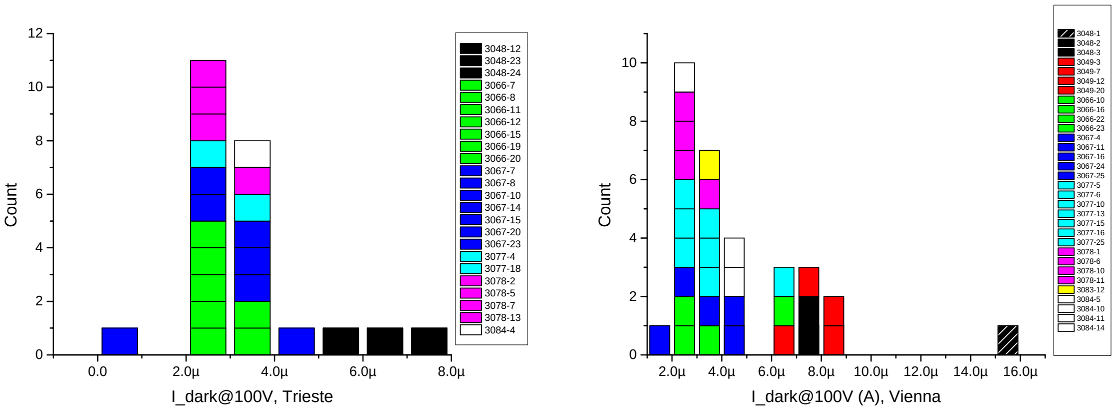

(a) Histogram of the dark current at 100 V, Trieste.

(b) Histogram of the dark current at 100 V, Vienna.

Figure 6.35.: Dark current of the sensors at 100 V, Trieste and Vienna.

The dark current should be higher if the strip currents are high. The sum of the strip currents is a low limit for the total leakage current. For sure if there are scratches the total leakage current will be higher. In any case we expect a relation between the values of the strip current and the total dark current. To support this assumption we calculated the Pearson's correlation coefficient between the mean single strip currents of the p-sides and the total leakage currents. To obtain better results we masked the outlier sensor 3048-1 which was completely outside the other results in the scatter diagram. The correlation coefficient was calculated between the mean values of the single strip currents of the p-side and the dark currents measured at 100 V. It is significant with r= 0.84 and an adjusted R-square of 0.70. Graph 6.36 shows the linear regression between the mean value $\bar{I}_{strip}$ and I_{dark}. The intercept is $1.13 \cdot 10^{-6}$ and the slope 1182.3. So if the mean value of the single strip current is 1 nA higher, the dark current at 100 V should increase by about 1.2 μ. We calculated the correlation coefficient equally for the correlation between the average single strip current on the n-side and the dark current at 100 V. After masking 4 outliers the correlation was calculated and a significant Pearson correlation of $r = 0.79$ could be found.

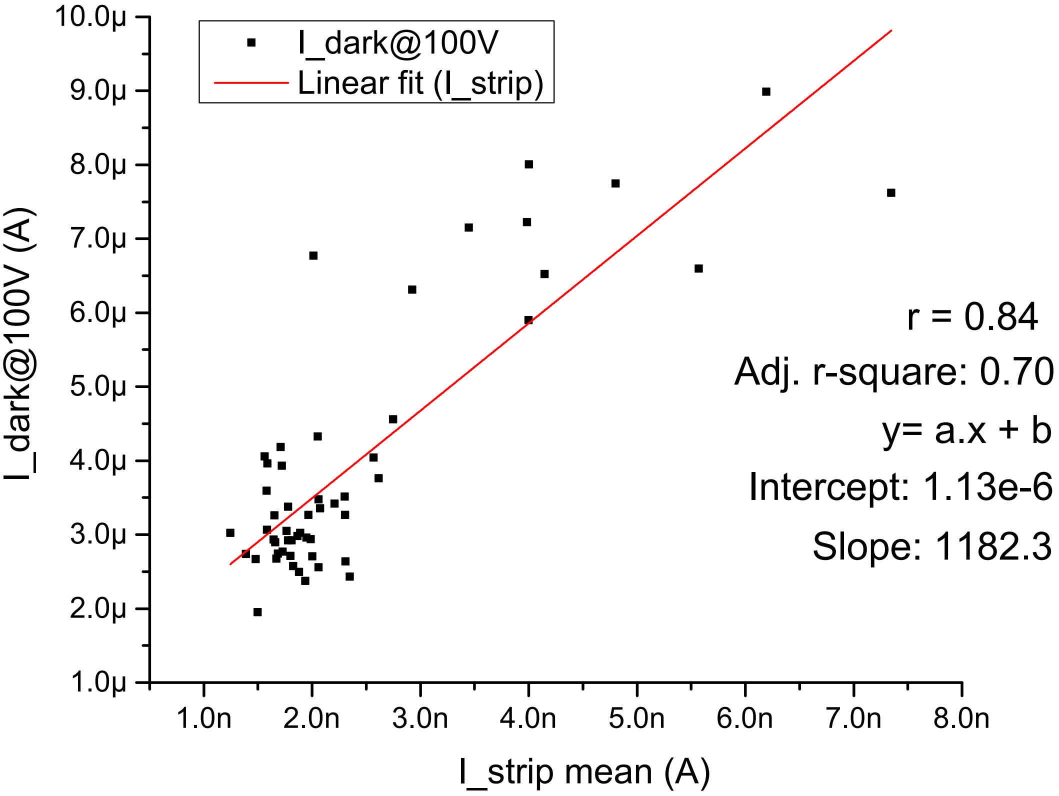

Figure 6.36.: Linear regression between $I_{strip,mean}$ and I_{dark}@100V.

6.8. Depletion voltage V_{depl}

By analyzing the CV-curves and fitting them with straight lines from the left and the right of the bend the depletion voltage was determined. Figure 6.37 (a) shows a histogram of all the depletion voltages measured. It can be seen that the first two batches (3048 and 3049) have a much smaller depletion voltage (between 20-25 V) than the rest of the sensors. This can be most likely explained by the fact that Micron Semiconductors used a different silicon ingot for the first two batches. For the rest of the sensors there

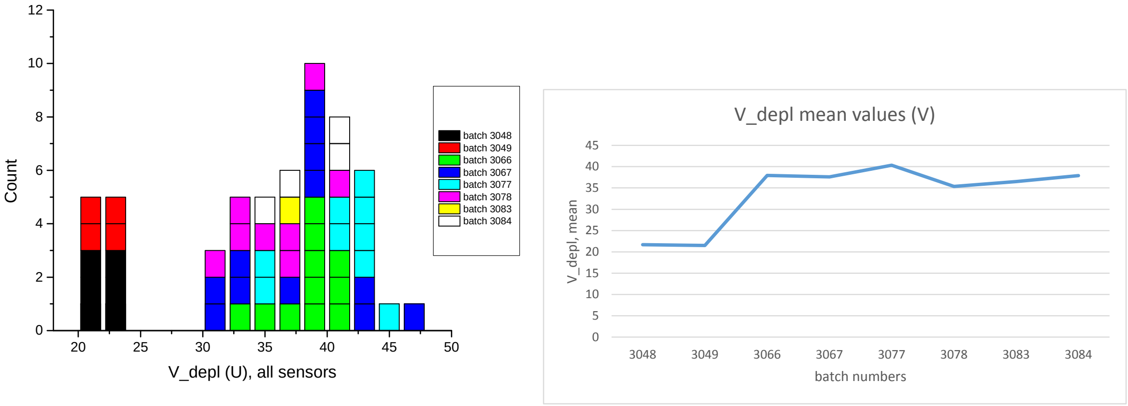

(a) Depletion voltage of all sensors measured, grouped by colors into the different batches.

(b) Graph of the mean values of the V_{depl} of the different batches.

Figure 6.37.: Distributions of the depletion voltage

is one peak for the depletion voltage between 38-40 V and the rest of the sensors are between 30-48 V. The difference in the mean values of the batches can also be seen in graph 6.37 (b). Because of the big differences between the early and the later batches two Gaussian fits were performed, one for the first two batches and one for the rest of the sensors. The Gaussian fits can be seen in figure 6.38. Both fits were not really satisfying, since the adjusted R-square is rather far away from the perfect value 1 with 0.76 respectively 0.62.

With the values of the depletion voltage the resistivity of the doped silicon can be calculated using formula 6.1. The unity of the resistivity is Ωcm. The lower the resistivity the better the conduction of a given semiconductor. In the given formula W is the width of the depleted area (300 μm), ϵ_0 is the vacuum permeability (8.85×10^{-12} As/Vm) and ϵ_r the relative permeability of silicon (11.9). μ is the mobility of the majority charge carriers (since we have an n-bulk electrons 1450 cm^2/Vs) and V is the full depletion voltage (so between 20 and 50 V).

$$W = \sqrt{2\epsilon_0\epsilon_r\mu\rho|V|} \tag{6.1}$$

Entering those values in the formula and expressing ρ in the formula results in resistivity values varying between 14.7 kΩcm for a depletion voltage of 20 V and 5.9 kΩcm for a depletion voltage of 50 V. The effective doping concentration can be estimated using formula 6.2, with e being the elementary charge ($1.6 \times 10^{-19} C$) and μ again the mobility of electrons. Entering those values in the formula results in a effective doping concentration varying between 1.2×10^{12} (for 50 V) and 5×10^{11} (for 20 V).

$$N_{eff} = \frac{1}{e\mu\rho} \tag{6.2}$$

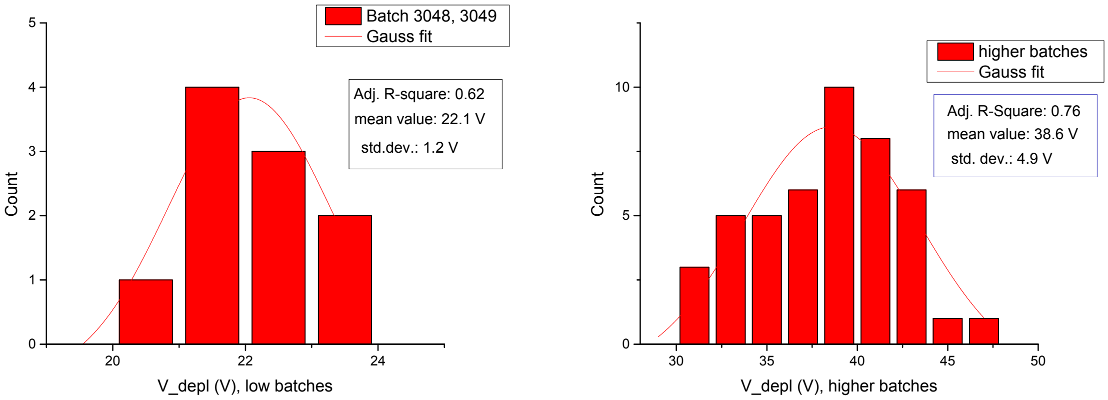

(a) Depletion voltages of sensor batch 3048 and 3049, fitted by a normal distribution

(b) Depletion voltages of the higher sensor batches (all except 3048 and 3049), fitted by a normal distribution.

Figure 6.38.: Gaussian fits of the depletion voltages.

6.9. Sensor grading

The 32 sensors measured in Vienna and the 24 sensors measured in Trieste were classified into three classes of quality. A is the best grade, B is average and C is the worst possible grade. The criteria for the grading were explained in chapter 5.3. The sensors from Micron were either accepted or rejected. The rejected sensors were mostly C rated but there are also some examples were B rated sensors were rejected (e.g. because they were too thin). There is also an example for a sensor that was accepted from Micron but C rated because it got a crack during the measurement process (3084-10). Of the 56 sensors in total, 6 sensors were rated with a C, 19 with a B and 31 with an A.

6.9.1. Vienna

Figure 6.39 shows the grades for the 32 sensors that were measured in Vienna. Of 32 shipped sensors, 9 were rejected which results in a percentage of 28.1 %. Two of them were rejected, because the dark current was too high. The sensor 3049-12 didn't perform well at the long term measurements in the climate chamber. At those measurements in the so-called climate chamber the sensors are reversely biased and then humidity is variated. The given sensor showed very unstable behavior, that's why it was rejected. The sensor 3067-11 was rejected because of random values of the coupling capacitance. The sensors 3067-25. 3078-6 and 3078-11 were rejected because they were too thin. Finally 3084-11 was rejected because it was badly diced. Of the 32 sensors measured in Vienna, 5 were rated with C, 12 with B and 15 with A.

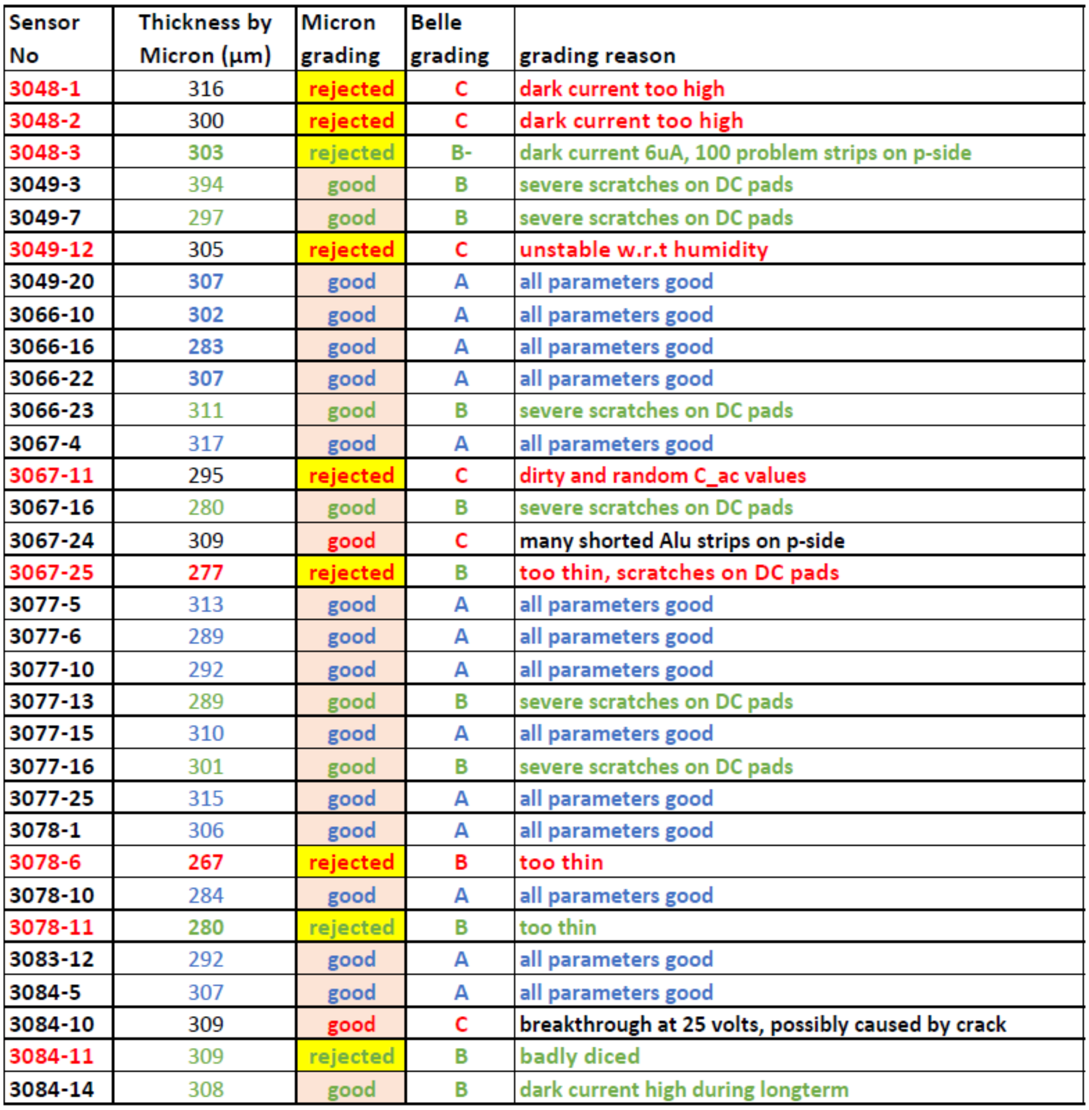

Sensor No	Thickness by Micron (µm)	Micron grading	Belle grading	grading reason
3048-1	316	rejected	C	dark current too high
3048-2	300	rejected	C	dark current too high
3048-3	303	rejected	B-	dark current 6uA, 100 problem strips on p-side
3049-3	394	good	B	severe scratches on DC pads
3049-7	297	good	B	severe scratches on DC pads
3049-12	305	rejected	C	unstable w.r.t humidity
3049-20	307	good	A	all parameters good
3066-10	302	good	A	all parameters good
3066-16	283	good	A	all parameters good
3066-22	307	good	A	all parameters good
3066-23	311	good	B	severe scratches on DC pads
3067-4	317	good	A	all parameters good
3067-11	295	rejected	C	dirty and random C_ac values
3067-16	280	good	B	severe scratches on DC pads
3067-24	309	good	C	many shorted Alu strips on p-side
3067-25	277	rejected	B	too thin, scratches on DC pads
3077-5	313	good	A	all parameters good
3077-6	289	good	A	all parameters good
3077-10	292	good	A	all parameters good
3077-13	289	good	B	severe scratches on DC pads
3077-15	310	good	A	all parameters good
3077-16	301	good	B	severe scratches on DC pads
3077-25	315	good	A	all parameters good
3078-1	306	good	A	all parameters good
3078-6	267	rejected	B	too thin
3078-10	284	good	A	all parameters good
3078-11	280	rejected	B	too thin
3083-12	292	good	A	all parameters good
3084-5	307	good	A	all parameters good
3084-10	309	good	C	breakthrough at 25 volts, possibly caused by crack
3084-11	309	rejected	B	badly diced
3084-14	308	good	B	dark current high during longterm

Figure 6.39.: Grading of the sensors tested in Vienna. Out of 32 measured sensors, 9 were rejected because of different reasons (w.r.t stands for with respect to).

6.9.2. Trieste

Figure 6.40 shows the grading of the 24 sensors that were measured in Trieste. Out of 24 tested sensors only 4 were rejected which results in a percentage of 16.7%. Two (3067-20 and 3067-15) because they were too thin, one (3078-2) because of more than 1% pinholes and one (3078-2) because it didn't perform well in the long term test in the climate chamber. In total, there were 7 sensors B-graded because of different reasons. Even though 4 sensors were rejected at Micron, only one sensor was C graded. Of the

24 sensors measured in Trieste, one was rated with C, 7 with B and 16 with A.

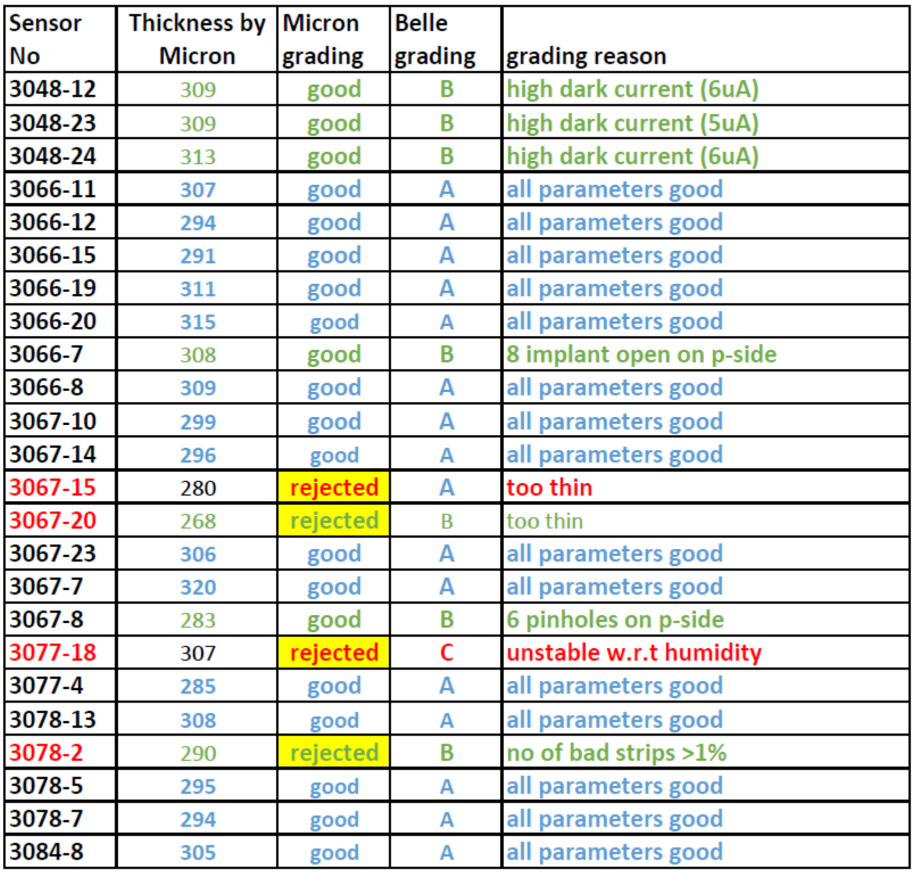

Sensor No	Thickness by Micron	Micron grading	Belle grading	grading reason
3048-12	309	good	B	high dark current (6uA)
3048-23	309	good	B	high dark current (5uA)
3048-24	313	good	B	high dark current (6uA)
3066-11	307	good	A	all parameters good
3066-12	294	good	A	all parameters good
3066-15	291	good	A	all parameters good
3066-19	311	good	A	all parameters good
3066-20	315	good	A	all parameters good
3066-7	308	good	B	8 implant open on p-side
3066-8	309	good	A	all parameters good
3067-10	299	good	A	all parameters good
3067-14	296	good	A	all parameters good
3067-15	280	rejected	A	too thin
3067-20	268	rejected	B	too thin
3067-23	306	good	A	all parameters good
3067-7	320	good	A	all parameters good
3067-8	283	good	B	6 pinholes on p-side
3077-18	307	rejected	C	unstable w.r.t humidity
3077-4	285	good	A	all parameters good
3078-13	308	good	A	all parameters good
3078-2	290	rejected	B	no of bad strips >1%
3078-5	295	good	A	all parameters good
3078-7	294	good	A	all parameters good
3084-8	305	good	A	all parameters good

Figure 6.40.: Grading of the sensors tested in Trieste. Out of 24 measured sensors, 3 were rejected.

7. Summary

In total 56 trapezoidal sensors that were produced by Micron Semiconductors were tested mechanically, optically and electrically. Of the in total 56 sensors measured, 32 of them were tested at the Quality Testing Center at HEPHY Vienna and 24 by our colleagues at INFN in Trieste. The most important parameters determined were the full depletion voltage, the total leakage current and the number and the position of the strips with pinholes. Also the single strip current, the poly silicon resistance and the coupling capacitance were determined for every strip. Of the in total 56 sensors delivered, 43 were accepted and 13 were rejected which results in a acceptance percentage 77% and a rejection percentage of 23%. While of the Viennese sensors 9 sensors and 28% were rejected, only 4, respectively 17% of the Trieste sensors were rejected. The sensors were picked out randomly and the difference in the rejection percentage is not expected to be due to the measurement methods in Vienna and Trieste, even though systematical differences in the two measurement methods could be proven (by a t-test) for the coupling capacitance on n- and p-side. The reasons for rejection were high dark currents, unstable tests in the climate chamber, too thin sensors, random coupling capacitance values and a too high number of pinholes.

The results of the IV curves (see section 6.1) were all in all satisfactory. Of the 32 Viennese sensors only two sensors had not satisfying IV curves. The Trieste sensors also showed good behavior except three sensors that had a rather high leakage current.

Also for the CV curves (see section 6.2) respectively the depletion voltage V_{depl} (see section 6.8) the measurement results were satisfying. The values ranged between 20 V and 48 V and thus did by far not exceed the arranged typical depletion voltage of 100 V.

The tests of the single strip current I_{strip} (see section 6.3) were in total satisfactory. None of the measured strips exceeded the specification value of 20 nA. Also both the distributions of the n-side and the p-side (for all 56 sensors) were successfully fitted with a Gauss curve, with a r-square value of 0.95 (p-side) respectively 0.97 (n-side).

For the measurement results of the poly silicon resistance R_{poly} (see section 6.4) there were rather high deviations of the specifications. The values reached between 5 and 50 MΩ, instead of the 10-20 MΩ that were arranged with Micron. Also the distributions (for both n- and p-side) were not homogeneous at all. Gauss fits were performed but weren't satisfactory in this case. The inhomogeneous results for this parameter might be explained by slight time variations of the doping time (of the poly silicon resistors) that result in high differences of the resistance for the poly silicon resistors. In any case it was shown that even very big poly resistors of 50 MΩ aren't a problem for the detector since they induce a maximal voltage drop of only 2.5 V.

Regarding the coupling capacitance C_{ac} (see section 6.5) the measurement results were satisfying. For the n-side the distributions for both Trieste and Vienna were very homogeneous and the Gauss fits were very accurate. For the p-side that was the case for the Trieste results, but in Vienna (expectedly due to contacting problems during the measurements) too many low values for a good Gauss fit were measured. There is one interesting feature concerning the coupling capacitance: By the means of a t-test a very significant difference between the Viennese and results of Trieste were determined. This means that the results were influenced by the measurement method. It is assumed that the parameters that lead to a difference in both the mean values and the standard deviations were the frequency and the amplitude that were both different in the experiments in Vienna and Trieste. It would be certainly interesting to further investigate the influence of those parameters in a future project work.

The results for the number of pinholes (see section 6.6) did not fulfill the strict specifications. For the n-side 7 sensors and for the p-side even 14 of the 56 sensors exceeded the first arranged limit of lower than 0.5% pinholes per sensor. Because a higher number of pinholes is not a big problem, the specifications were changed to <1% pinholes per sensor. Then, only 1 sensor exceeded the value for the n-side, but still 5 sensors for the p-side. In any case this wasn't a big deal, since the most important point is that there are not more than 5 pinholes on 128 consecutive strips (which was never the case) , because only in this case the whole readout chip doesn't work.

For the dark current at 100 V (see section 6.7) only one sensor passed over the arranged limit of 10 μA, which is a good result. There were indeed 11 sensors with a rather high leakage current between 5 and 10 μ that were therefore mostly rated with the mark B.

To summarize again the results of the rating process- of the 56 sensors in total, 6 were rated with the mark C, 19 were marked with a B and 31 with the mark A. In general it can be said that the later batches performed better than the first two batches (3048, 3049), where the high dark current was a big problem. Of the 56 sensors in total 13 were rejected and 43 accepted.

The sensors tested that fulfilled the quality requirements will be used in the future Belle II project. Together with the rectangular Hamamatsu sensors they will build the Silicon Vertex Detector. The quality management was necessary to ensure a functioning Silicon Vertex Detector in the experiment. As explained, the aim of the SVD will be to reconstruct the vertices of collided particles. It will be mostly the A graded sensors that will be used for the experiment, only in case of a lack of high quality sensors also B rated sensors will be used. The experiment will start in 2016 and will hopefully bring new discoveries in the area of particle physics.

8. Bibliography

[1] HEPHY, *Institute of High Energy Physics of the Austrian Academy of Sciences*, Nikolsdorfer Gasse 18, 1050 Wien, Austria (http://www.hephy.at/)

[2] *http://www.nobelprize.org/nobel_prizes/physics/laureates/2008/*, The Official Web Site of the Nobel Prize

[3] KEK, *High Energy Accelerator Research Organisation (Tsukuba, Ibaraki, Japan)*, http://www.kek.jp

[4] J.W. Flanagan (ed.) and Y. Ohnishi (ed.) *Letter of intent for KEK Super B Factory, Part III: Accelerator Design*, KEK report 04-4 (2004)

[5] I. Gfall, *Mechanical Design of the Belle II Silicon Vertex Detector* , Master thesis, University of Vienna (2012)

[6] A. Frankenberger, *Cooling of the Belle II SVD* , Master thesis, University of Vienna (2013)

[7] Z. Dolezal (ed.) and S. Uno (ed.), *Belle II Technical design report*, KEK Report 2010-1 (2010)

[8] *http://en.wikipedia.org/wiki/P-n_junction*

[9] M. Krammer, *Lecture notes: Grundlagen der Teilchendetektoren*, http://www.hephy.at/lehre/

[10] T. Bergauer et al., *Resolution studies on silicon strip sensors with fine pitch*, EUDET-Memo-2008-15, http://www.eudet.org/e26/e28/e615/e782/EUDET-Memo-2008-15.pdf

[11] *http://en.wikipedia.org/wiki/Normal_distribution*

[12] *http://de.wikipedia.org/wiki/Wölbung_(Statistik)*

[13] T. Bergauer, Design, Construction and Commissioning of the CMS Tracker at CERN and Proposed Improvements for Detectors at the Future International Linear Collider, PhD thesis, TU Wien, 2008.

[14] J. Rehak, Messung der physikalischen und elektrisch aktiven Dicke von Siliziumdetektoren, Bachelor thesis, Vienna University of Technology (2014)

A. Acknowledgements

I want to thank my father Rudolf de Cillia and my brother Nicolas de Cillia for their help and support throughout my whole studies. Particularly the first years and the last year was very time consuming and they always supported me as well as they could.

I want to thank my colleagues Allan Hummer, Andrej Kliman and Lukas Sölkner who I made the bachelor in Technical Physics with for their great ambition, endurance and team spirit. Without them finishing the bachelor wouldn't have been possible.

I want to thank Thomas Bergauer for his supervision in this master thesis and Wolfgang Treberspurg for the helpful discussions I had with him. I finally want to thank Professor Manfred Krammer for being my supervisor in this work.